

## Seismic cycle and rheological effects on estimation of present-day slip rates for the Agua Blanca and San Miguel-Vallecitos faults, northern Baja California, Mexico

Timothy Dixon,<sup>1</sup> Julien Decaix,<sup>1</sup> Fred Farina,<sup>1</sup> Kevin Furlong,<sup>2</sup> Rocco Malservisi,<sup>2</sup> Richard Bennett,<sup>3</sup> Francisco Suarez-Vidal,<sup>4</sup> John Fletcher,<sup>4</sup> and Jeff Lee<sup>5</sup>

Received 8 December 2000; revised 12 April 2002; accepted 17 May 2002; published 11 October 2002.

[1] Geodesy can be used to infer long-term fault slip rates, assuming a model for crust and upper mantle rheology. We examine the sensitivity of fault slip rate estimates to assumed rheology for the Agua Blanca and San Miguel-Vallecitos faults in northern Baja California, Mexico, part of the Pacific–North America plate boundary zone. The Agua Blanca fault is seismically quiet, but offset alluvial fans indicate young activity. Current seismicity is confined to the nearby San Miguel-Vallecitos fault, a small offset fault better aligned with plate motion. GPS measurements between 1993 and 1998 suggest that both faults are active, with a combined slip rate of 4–8 mm yr<sup>-1</sup> regardless of rheological model. However, slip rate estimates for the individual faults are sensitive to assumed rheology. Elastic half-space models yield 2–3 mm yr<sup>-1</sup> for the Agua Blanca fault, and somewhat faster rates for the San Miguel-Vallecitos fault, 2–4 mm yr<sup>-1</sup>, with uncertainties of about 1 mm yr<sup>-1</sup>. Models incorporating viscoelastic rheology and seismic cycle effects suggest a faster slip rate for the Agua Blanca fault, 6 ± 1 mm yr<sup>-1</sup>, and a slower rate for the San Miguel-Vallecitos fault, 1 ± 1 mm yr<sup>-1</sup>, in better agreement with geological data, but these rates are sensitive to assumed rheology. Numerical simulations with a finite element model suggest that for similar rheological and friction conditions, slip on the San Miguel-Vallecitos fault should be favored due to better alignment with plate motion. Long-term faulting processes in the larger offset Agua Blanca fault may have lowered slip resistance, allowing accommodation of motion despite misalignment with plate motion. *INDEX TERMS:* 1206 Geodesy and Gravity: Crustal movements—interplate (8155); 1236 Geodesy and Gravity: Rheology of the lithosphere and mantle (8160); 8107 Tectonophysics: Continental neotectonics; *KEYWORDS:* fault slip rates and the seismic cycle; northern Baja California

**Citation:** Dixon, T., J. Decaix, F. Farina, K. Furlong, R. Malservisi, R. Bennett, F. Suarez-Vidal, J. Fletcher, and J. Lee, Seismic cycle and rheological effects on estimation of present-day slip rates for the Agua Blanca and San Miguel-Vallecitos faults, northern Baja California, Mexico, *J. Geophys. Res.*, 107(B10), 2226, doi:10.1029/2000JB000099, 2002.

### 1. Introduction

[2] Long-term or geological fault slip rates can be determined from high precision geodetic techniques such as the Global Positioning System (GPS) with the use of a rheological model of the Earth that relates measured elastic (recoverable) displacement within an earthquake cycle to longer term displacement averaging over many seismic

cycles. If the assumed rheology is a poor representation of reality, geodetic data may fit a given model, but the slip rate estimate may be wrong. Simple elastic half-space models [Savage and Burford, 1973; Okada, 1985, 1992] are often used, since they fit a variety of geodetic data and are easy to implement. For a more realistic layered Earth model, with an elastic upper crust above one or more viscous or viscoelastic layers, present-day surface velocities measured near active faults may be influenced by past earthquakes. These effects can extend far from the fault and persist long after the last earthquake, depending on earthquake history, fault depth, and crustal and upper mantle rheology [e.g., Savage and Prescott, 1978; Thatcher, 1983; Li and Rice, 1987; Savage and Lisowski, 1998]. While these models are more difficult to implement, they may give a more accurate estimate of long-term fault slip rate.

[3] We present preliminary site velocity data from a GPS network around the Agua Blanca and San Miguel-Vallecitos faults in northern Baja California, Mexico, part of the active Pacific–North America plate boundary zone (Figure 1), and

<sup>1</sup>Rosenstiel School for Marine and Atmospheric Sciences, University of Miami, Florida, USA.

<sup>2</sup>Geodynamics Research Group, Department of Geosciences, Pennsylvania State University, University Park, Pennsylvania, USA.

<sup>3</sup>Harvard-Smithsonian Center for Astrophysics, Cambridge, Massachusetts, USA.

<sup>4</sup>Centro de Investigación Científica y Educación Superior de Ensenada, Ensenada, Baja California, Mexico.

<sup>5</sup>Department of Geological Sciences, Central Washington University, Ellensburg, Washington, USA.

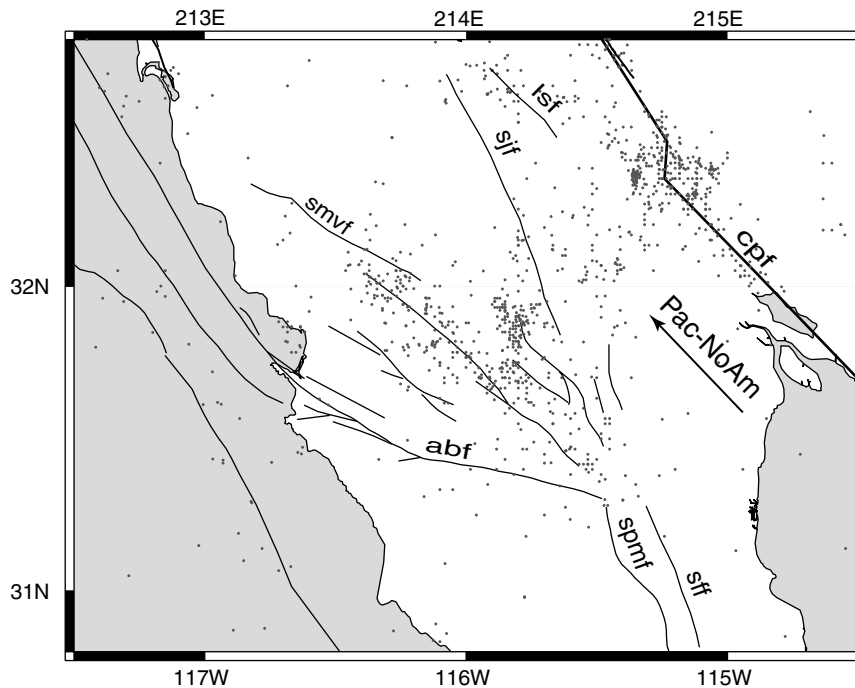


**Figure 1.** Seismicity and major known faults in northern Baja California, Mexico. Earthquake data from US Geological Survey Earthquake Information Center, incorporating all events in the data base above 60 km depth from January 1967 to November 1998. Fault names are: abf (Agua Blanca fault), cpf (Cerro Prieto fault), lsf (Laguna Salada fault), sjf (Sierra Juarez fault), smvf (San Miguel-Vallecitos fault), and spmf (San Felipe fault). The Cerro Prieto fault (bold line) is the main plate boundary fault. Arrow shows approximate direction of Pacific–North America plate motion, from geological model of *DeMets and Dixon [1999]*.

examine the sensitivity of the resulting fault slip rate estimates to the choice of rheological model. We also examine the influence of other analytical choices (e.g., reference frame, inclusion or exclusion of individual data), and discuss implications for neotectonics and seismic hazard in the region.

## 2. Geological Background and Previous Work

[4] The Agua Blanca fault is a major right lateral strike-slip fault spanning the northern Baja California peninsula (Figure 1), with total offset exceeding 15 km [*Allan et al., 1960*]. This fault probably became active as a result of the plate boundary jump from offshore North America to its present position in the Gulf of California at about 3.5–5.5 Ma [*Atwater, 1970, 1989*]. Offset Quaternary alluvial fans indicate relatively young activity on the fault [*Suarez-Vidal et al., 1991*], but the present rate of motion, and indeed whether the fault is currently active, are poorly known. Seismicity is largely confined to the San Miguel-Vallecitos fault to the north [*Rebollar and Reichle, 1987; Figure 1*]. However, total offset on this fault is less than about 500 m, suggesting that it is a very young feature, and/or its long-term slip rate is very low [*Hirabayashi et al., 1996*]. Because this fault is better aligned with the current Pacific–North America plate motion direction [*DeMets and Dixon, 1999*], one possibility is that the Agua Blanca fault has been recently abandoned, with slip taken up on the newly formed San Miguel-Vallecitos fault. Alternately, the

Agua Blanca fault is currently locked and accumulating strain, to be released in a future earthquake. Distinguishing between these scenarios is not straightforward. Assuming both faults are active, their strain fields overlap, and they may be in different stages of their earthquake cycle. In this case, slip rates estimated from surface deformation data may be sensitive to the assumed rheological model.

[5] *Bennett et al. [1996]* used GPS data to infer long-term slip rates of  $4 \pm 3$  and  $3 \pm 3$  (one standard error) for the Agua Blanca and San Miguel-Vallecitos fault zones, respectively, employing an elastic half-space model that accounts for the geometric effects of nonparallel faults. The portion of their network spanning the Agua Blanca and San Miguel-Vallecitos fault zones was quite sparse (e.g., only one site south of the Agua Blanca fault), consequently details of the strain accumulation pattern around the faults and possible earthquake cycle effects could not be investigated.

## 3. Observations and Data Analysis

[6] GPS data were obtained from campaign observations at 15 sites in 1993, 1994, 1995 and 1998, and from the semipermanent, continuously recording station at Ensenada (CICE) which we installed in 1995 (Figures 2 and 3; Tables 1, 2, and 3). Campaign site velocities reported here are based on data spanning the full five years and acquired in at least three separate years, but not all sites were occupied in 1994 and 1995 (Figure 2). During an occupation, most sites were observed for 24 hours per day for 3–5 days.

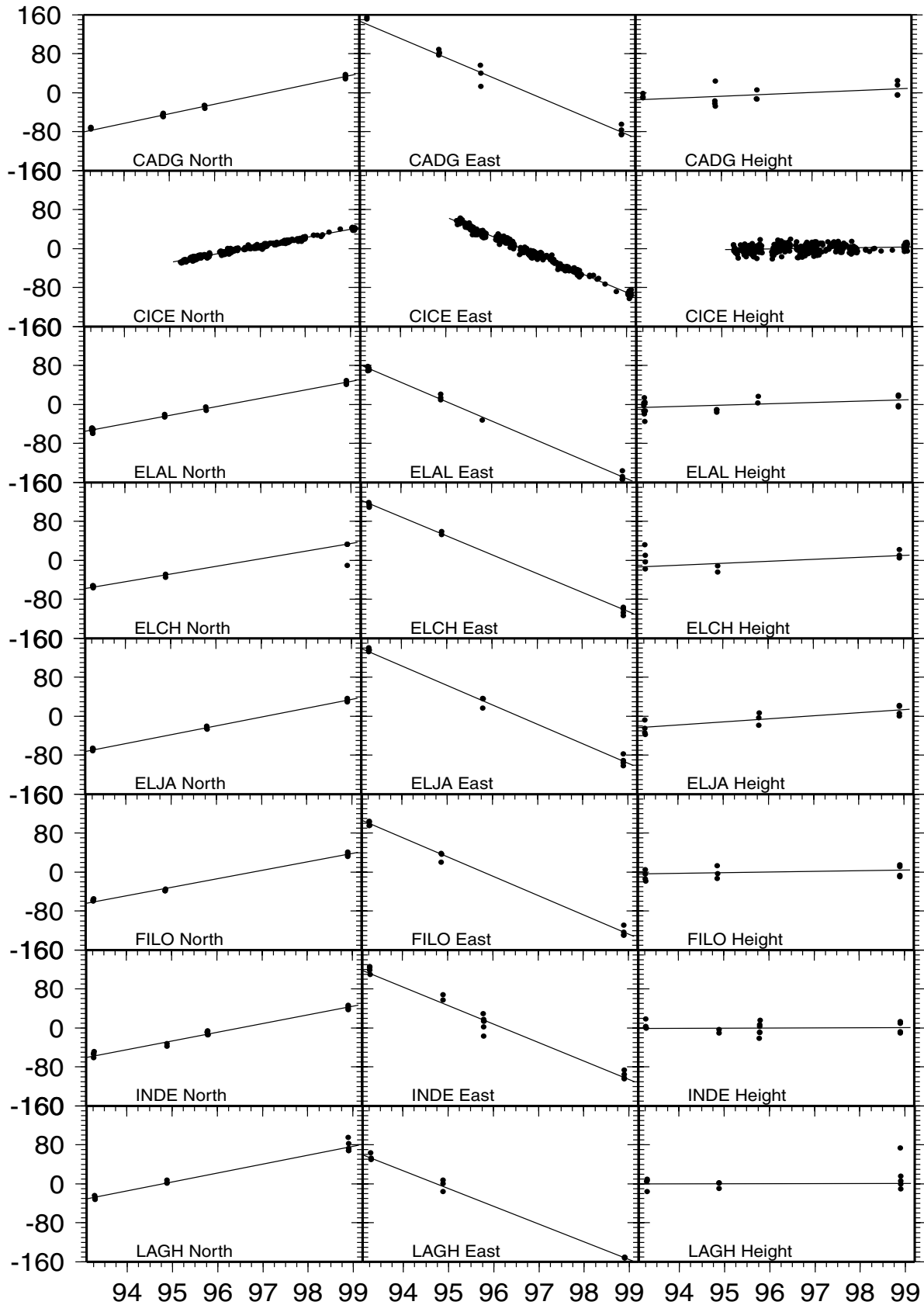


**Figure 2.** GPS site position estimates for 1993–1998, relative to ITRF-96, minus an arbitrary constant. Site velocity (Table 1) is given by a weighted least squares line through these data. Error bars omitted for clarity.

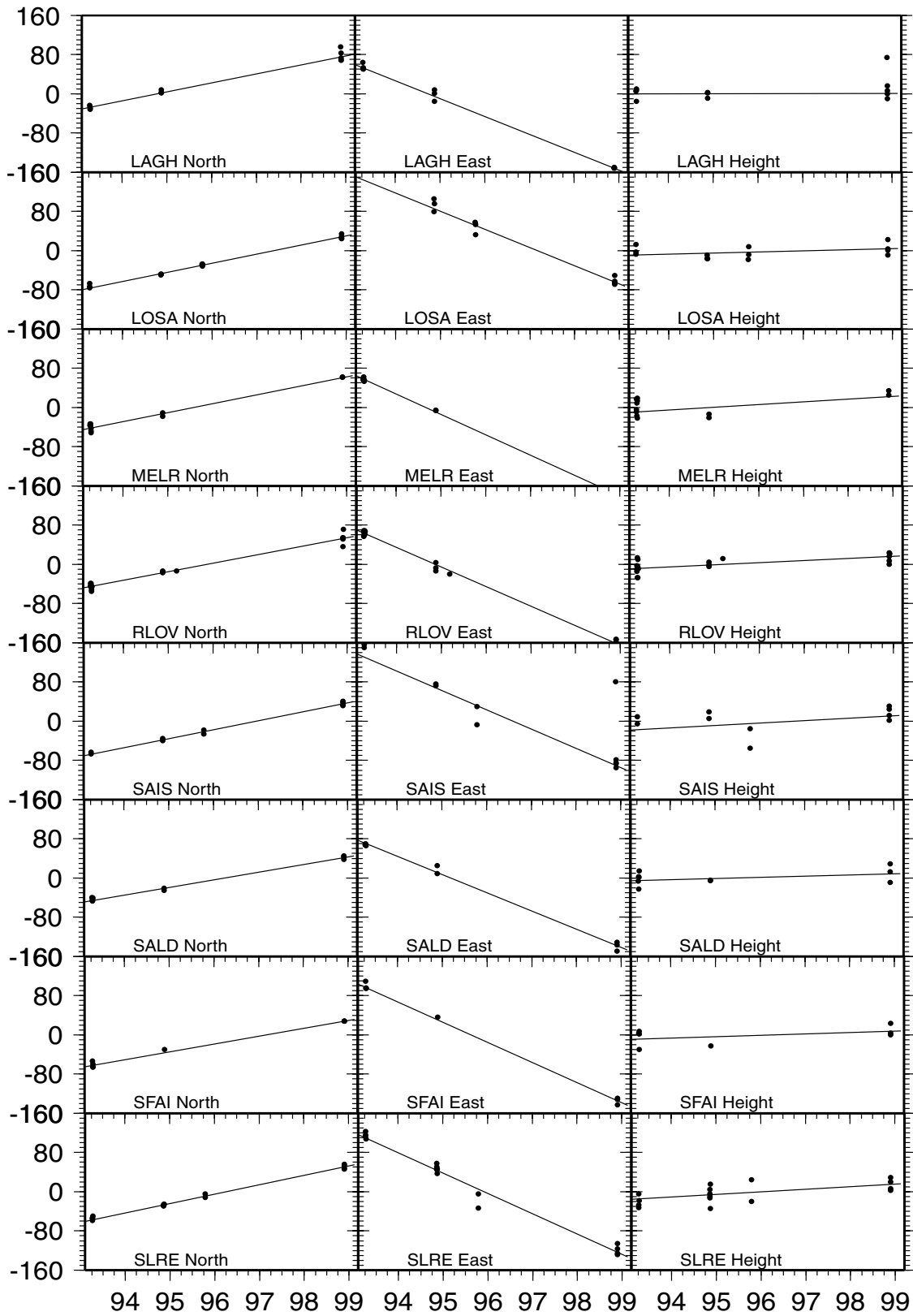
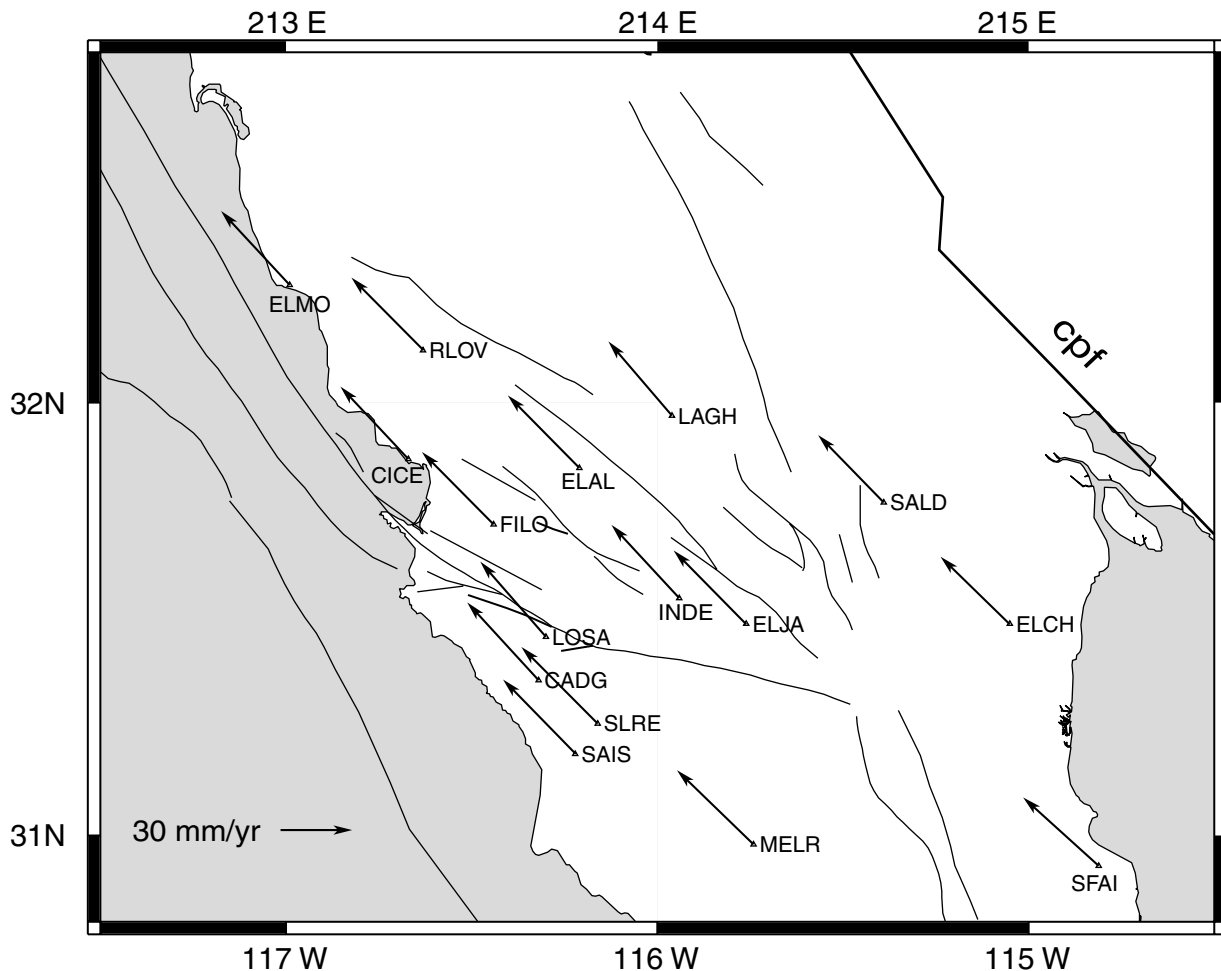


Figure 2. (continued)



**Figure 3.** GPS site locations, names, and velocity data relative to stable North America based on coordinate solutions (Table 2). Sites LOSA, CADG, SLRE and SAIS south of the Agua Blanca fault were occupied simultaneously with either ELAL, FILO or ELJA north of the fault to form a relative velocity transect (Table 3; Figure 4). Plate motion direction is indicated approximately by strike of Cerro Prieto fault (cpf). 95% confidence ellipses for velocity vectors are smaller than arrowheads.

[7] We report site velocities based on both coordinate (“absolute”) positions and more precise relative position data where available. In most campaigns, a subset of sites was occupied simultaneously, defining a transect across the Agua Blanca fault relative to a reference site. For some applications these relative position data are more precise than coordinate data because orbit and atmospheric effects, major noise sources in GPS, are common mode and largely cancel for closely spaced sites observed simultaneously. A generalization of this technique may be used where a dense network of sites with continuous observations is locally available, allowing reduction of common mode errors in the region without relying on a single reference site [Wdowinski *et al.*, 1997]. Unfortunately such a network was not available during the most of the observation period.

[8] The transect consists of 4 sites south of the fault (SAIS, SLRE, CADG, LOSA) and one site north of the fault (ELAL), arbitrarily taken as the reference site. Some data from two other sites north of the fault (ELJA, FILO) were also acquired simultaneously, allowing tests of the effect of different reference sites. Sites spanning the San Miguel-

Vallecitos fault were not observed simultaneously, hence only coordinate velocities are available.

[9] The 1993 campaign occurred in April, while the remainder of the campaigns occurred in October–November. Thus the possibility exists that the coordinate velocities are affected by seasonal or annual processes, whose effects on the coordinate velocity estimates may be amplified for campaign observations acquired at different times of the year (the effects are less important for short baseline relative velocities). Based on results from the continuous site CICE (Figure 2), annual effects appear to be small and are ignored here.

[10] We also used observations from 16 continuously recording stations distributed through eastern and central North America, operated by various agencies, to define a stable North America reference frame, as outlined by Dixon *et al.* [1996] and DeMets and Dixon [1999].

[11] Data were analyzed at the University of Miami following Dixon *et al.* [1997]. Briefly, we used the GIPSY software developed at the Jet Propulsion Laboratory (JPL) and satellite ephemeris and clock files provided by JPL

**Table 1.** GPS Velocities Relative to ITRF-96 and Weighted RMS Scatter

Site	Latitude	Longitude	$\Delta T$	$N$	Velocity, mm yr <sup>-1</sup>			WRMS, mm		
					North	East	Vertical	North	East	Vertical
CADG	31.36	243.68	5.6	14	19.6 ± 1.0	-39.3 ± 3.6	3.8 ± 3.5	3.6	14.3	13.9
CICE	31.87	243.33	3.7	1246	17.5 ± 0.6	-38.0 ± 0.9	1.5 ± 2.0	2.4	4.6	7.6
ELAL	31.85	243.79	5.6	18	17.4 ± 1.0	-39.5 ± 1.2	2.6 ± 3.3	3.8	5.3	13.2
ELCH	31.49	244.95	5.6	10	15.7 ± 0.8	-38.6 ± 1.3	4.0 ± 4.5	2.6	4.9	17.2
ELJA	31.49	244.24	5.6	11	18.1 ± 0.9	-39.9 ± 2.6	6.4 ± 3.2	3.1	10.0	11.4
ELMO	32.27	243.01	5.6	15	17.9 ± 0.9	38.4 ± 1.4	1.4 ± 2.7	3.4	5.6	9.4
FILO	31.72	243.56	5.6	11	17.3 ± 1.1	-39.5 ± 1.7	1.4 ± 3.2	3.7	6.6	11.5
INDE	31.55	244.06	5.6	16	17.8 ± 1.4	-37.9 ± 3.5	0.3 ± 2.8	5.1	14.6	10.3
LAGH	31.97	244.04	5.6	12	18.3 ± 1.0	-36.3 ± 1.7	0.2 ± 2.9	3.4	6.6	10.0
LOSA	31.46	243.70	5.6	14	18.6 ± 1.0	-37.0 ± 3.1	2.3 ± 3.2	3.6	12.3	12.3
MELR	30.98	244.26	5.6	12	18.3 ± 1.3	-41.5 ± 1.0	5.5 ± 4.3	4.5	3.7	17.0
RLOV	32.12	243.37	5.6	18	17.4 ± 0.8	-39.8 ± 1.4	4.3 ± 2.9	3.0	6.1	11.1
SAIS	31.19	243.78	5.6	11	18.3 ± 1.2	-39.3 ± 4.5	4.9 ± 6.8	4.2	17.3	28.6
SALD	31.77	244.61	5.6	10	15.5 ± 1.1	-37.1 ± 2.0	2.4 ± 3.7	3.6	7.6	13.3
SFAI	30.93	245.19	5.6	8	16.1 ± 0.8	-41.1 ± 1.5	2.9 ± 4.4	2.6	5.4	15.5
SLRE	31.26	243.84	5.6	16	19.2 ± 0.8	-41.4 ± 3.6	5.3 ± 3.6	3.1	14.8	14.7

[Zumberge *et al.*, 1997], deriving daily position estimates in global reference frame ITRF-96 [Sillard *et al.*, 1998]. Velocity estimates and the weighted root mean square scatter (WRMS), a measure of data quality, are based on a weighted least squares line fit to the position data (Table 1; Figure 2). For the subset of data on stable North America, we used a formal inversion to derive a best fit angular velocity vector describing motion of North America. The resulting North America reference frame is essentially identical to that described by *DeMets and Dixon* [1999] but an additional 6 months of data were incorporated. Velocities of the northern Baja California sites are reported relative to this definition of stable North America (Table 2). We can test the integrity of this reference frame by comparing its velocity predictions along the Pacific–North America plate boundary to the predictions of an independently derived geological model [DeMets and Dixon, 1999]. The two velocities agree to better than 1.5 mm yr<sup>-1</sup> throughout the region of interest, about the level expected from uncertainties.

[12] Velocity errors are estimated following *Mao et al.* [1999] and account for the influence of white (uncorrelated in time) and colored (time-correlated) noise, as well as individual station variations, based on an assumed relation between WRMS and the magnitudes of white and flicker noise [Dixon *et al.*, 2000]. Correlations between north and east velocity uncertainties are small and are ignored. Unless specifically stated, all uncertainties in the tables and text represent one standard error, while error ellipses in figures represent two-dimensional 95% confidence regions (2.45 times the one-dimensional one standard error listed in Table 2).

[13] Several sites have relatively high scatter (high WRMS) in the east component, and correspondingly higher velocity errors (Tables 1 and 2), mainly reflecting higher scatter in the 1995 observations (e.g., CADG, INDE in Figure 2). While we have no explanation for the larger scatter in 1995, we note that it lies in the middle of the observation time span (1993–1998) and thus has only a small effect on the velocity estimates (the slope estimate is more sensitive to data at the beginning and end of the time series). Our velocity error model does not take this into

account, and thus may give somewhat conservative error estimates for these stations.

[14] The error estimates for the relative velocity data may also be conservative, since the error model is derived for coordinate time series, whose errors are dominated by orbit and atmospheric effects. These errors are common mode and largely cancel for simultaneous observations on nearby sites (monument noise is not common mode and does not cancel, though its effect may be small for these bedrock sites).

[15] *Bennett et al.* [1996] present velocities for six sites (SIO1, ENDA, LLCO, LPUR, MAYO and SM01) relevant to this study. Site velocities at three collocated sites (SIO1, CICE/ENDA SLRE/LLCO) overlap within uncertainties, but the *Bennett et al.* [1996] results are systematically faster (by an average 3.4 mm yr<sup>-1</sup>) compared to the current results, probably because of differences in how the North America reference frame is defined in the two studies. For estimation of fault slip rates, we are mainly interested in velocity gradients rather than “absolute” velocities, so reference frame differences are not critical. For this study, we simply adjusted the velocities of the three noncollocated sites (LPUR, MAYO and SMO1) by 3.4 mm yr<sup>-1</sup> to make

**Table 2.** GPS Velocities Relative to Stable North America

Site	North	East
CADG	32.57 ± 1.1	-29.88 ± 3.6
CICE	30.37 ± 0.7	-28.49 ± 1.0
ELAL	30.34 ± 1.1	-29.94 ± 1.3
ELCH	28.29 ± 1.0	-29.00 ± 1.4
ELJA	30.90 ± 1.1	-30.38 ± 2.7
ELMO	31.07 ± 1.1	-28.83 ± 1.5
FILO	30.31 ± 1.2	-30.00 ± 1.8
INDE	30.66 ± 1.4	-28.38 ± 3.6
LAGH	31.16 ± 1.1	-26.68 ± 1.8
LOSA	31.57 ± 1.1	-27.55 ± 3.1
MELR	31.10 ± 1.4	-32.10 ± 1.1
RLOV	30.46 ± 1.0	-30.22 ± 1.5
SAIS	31.24 ± 1.3	-29.91 ± 4.6
SALD	28.19 ± 1.2	-27.46 ± 2.1
SFAI	28.61 ± 1.0	-31.61 ± 1.6
SLRE	32.12 ± 1.0	-31.98 ± 3.6

**Table 3.** Global Positioning System Baseline Velocities

Site	North	East	Vertical	WRMS N	WRMS E	WRMS V
<i>GPS Site Velocities Relative to ELAL</i>						
CADG	1.8 ± 0.7	-1.8 ± 1.6	0.7 ± 3.	1.0	2.5	5.3
LOSA	0.9 ± 1.1	-1.5 ± 2.5	-2.4 ± 4.3	1.1	2.0	9.2
SAIS	1.1 ± 0.8	-2.2 ± 1.9	0.5 ± 4.4	0.5	4.2	4.6
SLRE	1.8 ± 0.6	-2.1 ± 1.4	4.2 ± 3.2	1.0	4.1	9.1
<i>GPS Site velocities relative to FILO</i>						
CADG	1.9 ± 0.6	-1.6 ± 1.5	3.1 ± 3.3	1.8	2.8	12.0
LOSA	1.0 ± 0.7	-0.9 ± 1.9	0.4 ± 3.7	1.3	3.4	13.2
SAIS	1.1 ± 0.6	-1.6 ± 1.6	1.4 ± 3.7	0.7	4.9	5.6
SLRE	1.6 ± 0.5	-2.0 ± 1.3	5.6 ± 3.0	2.0	4.9	10.0
<i>GPS Site velocities relative to ELJA</i>						
CADG	0.9 ± 0.8	-1.0 ± 1.9	-3.6 ± 4.1	1.1	2.5	7.2
LOSA	0.4 ± 1.3	-0.4 ± 2.7	-7.6 ± 4.8	1.3	3.8	11.9
SAIS	0.0 ± 0.9	-1.9 ± 2.2	-2.3 ± 5.1	1.0	6.9	6.9
SLRE	0.9 ± 0.7	-1.1 ± 1.6	-0.4 ± 3.6	2.1	3.1	6.7

the two sets of velocities consistent. Two models presented below compare results with and without these additional data. Analysis of the combined data set is currently underway.

#### 4. Data Results

[16] Velocity data relative to ITRF-96 are listed in Table 1, based on the position time series in Figure 2. Horizontal velocity components relative to stable North America are listed in Table 2 and plotted in Figure 3. Relative velocities for the Agua Blanca transects are listed in Table 3 and shown in Figure 4.

[17] The coordinate velocities define a velocity gradient of about 5 mm yr<sup>-1</sup> across the 110 km width of the study area, measured perpendicular to plate motion. The relative velocity data define a velocity difference across the Agua Blanca fault of about 2.5 mm yr<sup>-1</sup>, in a direction consistent with right lateral motion, i.e., sites south of the fault move west-northwest relative to a given reference site north of the fault. Thus, lack of seismicity on the Agua Blanca fault can be interpreted in the context of an active fault that is locked and accumulating elastic strain, to be released in a future earthquake.

[18] The Agua Blanca fault strikes as much as 25° oblique to the plate motion direction. In a local reference frame defined by the relative position data (Table 3), appropriate for considering local fault motion, the average relative velocity for the four sites south of the Agua Blanca fault relative to ELAL immediately north of the fault is 13° oblique to fault strike. For the range of fault slip rates derived later in this report, this translates into less than 1.5 mm yr<sup>-1</sup> of convergence normal to the fault. In one of the models to be discussed, motion perpendicular to the Agua Blanca fault is explicitly estimated at 0.5 ± 0.9 mm yr<sup>-1</sup>, small compared to the fault-parallel component. Thus, despite its obliquity, the dominant faulting mode on this fault is strike-slip.

#### 5. Model Results

[19] We compare fault slip rate estimates based on three modeling strategies:

1. A simple analytical forward model that assumes elastic half-space rheology and one, two or three infinitely long, parallel faults;

2. A block model that also assumes elastic half-space rheology but accounts for finite length, nonparallel fault geometry, implemented with an inverse approach;

3. An analytical forward model involving an elastic layer over a viscoelastic half-space, assuming two, three or four infinitely long, parallel faults.

[20] We also present preliminary results from a finite element model designed to investigate some aspects of fault interaction and dynamics.

[21] Fault slip rate models are evaluated with the  $\chi^2$  statistic, describing data misfit for a given model:

$$\chi^2 = \sum_{i=1}^N \frac{(O_i - C_i)^2}{\sigma_i^2} \quad (1)$$

where  $O_i$  is a velocity observation (north, east, or rate),  $C_i$  is the calculated velocity at the same site,  $\sigma_i$  is the velocity error, and  $N$  is the number of data. The minimum  $\chi^2$  indicates the best fit model. In its normalized form,  $\chi^2_\nu$ , (1) is divided by the number of degrees of freedom,  $N-\nu$ , where  $\nu$  is the number of adjustable parameters. Values of  $\chi^2_\nu \sim 1.0$  indicate a good fit of data to model and suggest that error estimates are reasonable.  $\chi^2_\nu < 1.0$  suggest that errors are overestimated, while  $\chi^2_\nu > 1.0$  suggest either that errors are underestimated or that a given model poorly fits the data. Since our sample size is small, this rule of thumb is only a rough guide.

[22] The major plate boundary fault in this region is the Cerro Prieto fault (Figure 1). High heat flow and shallow earthquake epicenters near this fault are generally interpreted as evidence for a shallow locking depth [e.g., *Bennett et al.*, 1996], limiting the fault's influence on the regional strain field. We ran models both with and without the Cerro Prieta fault, but since our data do not span this feature, most models discussed below exclude it.

##### 5.1. Parallel Faults in an Elastic Half-Space

[23] For three locked, parallel strike-slip faults in an elastic half-space, the velocity field in a reference frame

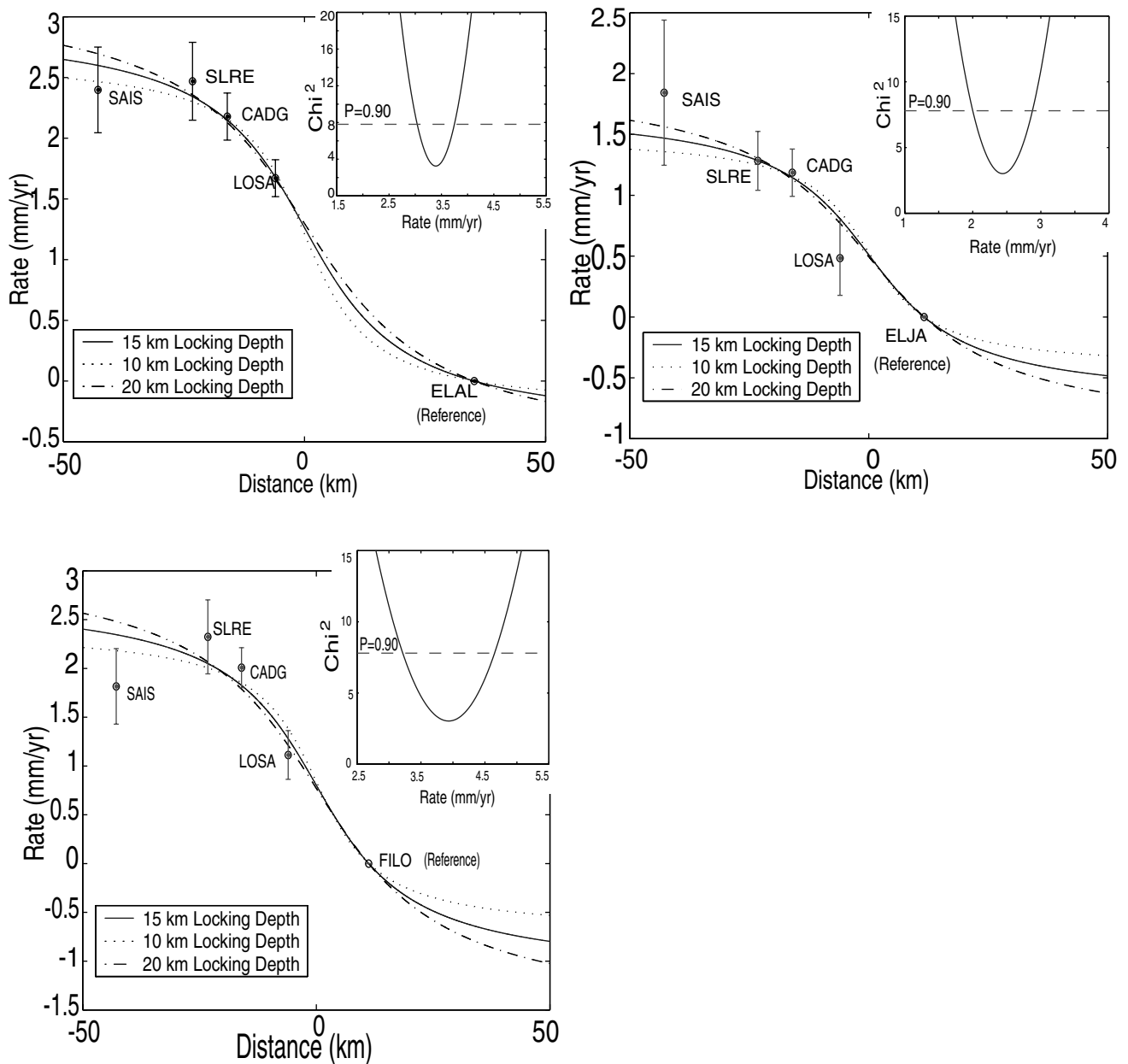


**Figure 4.** Relative velocity data for transects across the Agua Blanca fault with ELAL, ELJA and FILO reference stations, and best fit elastic half space models for a single fault, with 15 km locking depth (solid line) and 10 and 20 km locking depth (dashed or dotted lines). Insets show  $\chi^2$  misfit for 15 km model as a function of slip rate. Line  $P = 0.90$  represents the probability that random errors could result in a value of  $\chi^2$  less than or equal to the specified value, assuming that errors are normally distributed and the model is appropriate. This is used to approximate one standard error limits for the slip rate estimates in Table 4, after normalizing the rate errors such that reduced  $\chi^2 = 1.0$  for each transect, to insure consistency among the three transects ( $\chi^2$  values before normalization are listed in Table 4).

defined by the perpendicular distance from the first fault is given by:

$$v = 1/\pi \{ v_{0,a} \tan^{-1}[x/D_a] + v_{0,b} \tan^{-1}[(x - S_b)/D_b] + v_{0,c} \tan^{-1}[(x - S_c)/D_c] \} \quad (2)$$

where  $v$  is the velocity at perpendicular distance  $x$  from the first fault ( $a$ ),  $v_{0,a}$ ,  $v_{0,b}$  and  $v_{0,c}$  are the far field fault velocities with locking depths  $D_a$ ,  $D_b$  and  $D_c$ , respectively, and  $S_b$  and

$S_c$  are the distance of the second and third faults respectively from the first fault [Savage and Burford, 1973; Dixon et al., 1995]. The model is easily expanded to account for additional faults. We first apply this model to a single (Agua Blanca) fault ( $v_{0,b} = 0$ ,  $v_{0,c} = 0$ ) using the precise relative position data. We then investigate the influence of the San Miguel-Vallecitos and Laguna Salada faults in two- and three-fault models by combining baseline and coordinate velocity data in a North America-fixed reference frame. In the latter case, we fix the velocity and locking depth of

**Table 4.** Slip Rate Estimates for Single and Multiple Parallel Fault, Elastic Half-Space Models

	AB, mm yr <sup>-1</sup>	SMV, mm yr <sup>-1</sup>	$\chi^2$	$\chi_v^2$
<i>Single-Fault Model (5 data, AB only)<sup>a</sup></i>				
Reference station				
FILO	3.9 ± 0.7	–	2.73	0.68
ELJA	2.4 ± 0.4	–	1.16	0.29
ELAL	3.4 ± 0.3	–	0.38	0.10
<i>Two-Fault Model (12 Data)<sup>a</sup></i>				
	2.9 ± 1.3	3.8 ± 1.1	7.7	0.77
<i>Three-Fault Model (15 or 12 Data)<sup>a,b</sup></i>				
15 data	2.3 ± 1.3	4.3 ± 1.1	10.5	0.81
12 data	3.1 ± 1.3	3.5 ± 1.1	7.8	0.78

AB is Agua Blanca fault, SMV is San Miguel-Vallecitos fault.

<sup>a</sup>Single-fault model for baseline data (Table 3) in three transects (Figure 4). Multiple-fault models use these data plus coordinate data in Table 2.

<sup>b</sup>Three-fault model assumes slip rate of 6 mm yr<sup>-1</sup> for Laguna Salada fault [Bennett *et al.*, 1996] and estimates rates for AB and SMV faults. Solution based on 15 data uses 12 data from this study and three data from Bennett *et al.* [1996].

the Laguna Salada fault based on independent data and estimate the velocities for the Agua Blanca and San Miguel-Vallecitos fault.

[24] When the error model described above is applied to the relative position data and the single-fault, elastic half-space models for the Agua Blanca fault,  $\chi_v^2 \ll 1$  (Table 4) suggesting that these errors may be overestimated. To obtain consistent uncertainties for the slip rates with these single-fault models, we adjusted the relative velocity errors such that on average  $\chi_v^2 = 1.0$ , reducing these errors by a factor of 2.7.

[25] Figure 4 shows the fault-parallel rate components of the velocities and adjusted errors for available sites relative to the three reference stations, and best fit single-fault, elastic half-space models for three locking depths (10, 15 and 20 km). The results are not strongly dependent on locking depth, and we take the result for 15 km as representative. Table 4 lists the corresponding slip rate estimates. Of the three transects, only the ELAL transect has an orientation that is close to orthogonal to the fault, has station locations that are all close to the transect (maximum orthogonal projection distance 10 km), and spans a considerable distance north of the fault.

[26] The  $\chi^2$  misfit function is also plotted in Figure 4 as a function of model slip rate. The minimum misfit solution, from the optimally oriented ELAL transect, is 3.4 ± 0.3 mm yr<sup>-1</sup>. The relative velocity data fit this simple model quite well: the RMS misfit for the four nonreference stations (by definition the reference station has zero misfit) is 0.12 mm yr<sup>-1</sup>. The RMS misfits for the other transects are 0.25 mm yr<sup>-1</sup> (ELJA reference) and 0.32 mm yr<sup>-1</sup> (FILO reference). The weighted mean of these slip rate estimates, and their RMS scatter about the weighted mean, is 3.1 ± 0.6 mm yr<sup>-1</sup>. We take this as the best estimate for the Agua Blanca slip rate and its uncertainty for the single-fault elastic half-space model.

[27] The reference stations for these transects (ELAL, ELJA, FILO) lie within the elastic strain field of the San Miguel-Vallecitos fault. Their velocities are affected in such a way as to overestimate the slip rate on the Agua Blanca

fault if this effect is ignored. To account for this, we used equation (2), solving for the slip rate of each fault assuming simple two- and three-fault models. We first combined the fault-parallel rate components of the relative velocities (ELAL transect) and most of the remaining coordinate velocities to generate a velocity profile perpendicular to the plate motion direction through the centroid of the network, using sites up to 70 km from the profile, for a total of 12 rate data, omitting SFAI to the southeast and ELMO, RLOV and CICE to the northwest (Figure 3). We assume that the absolute velocity of the reference site (e.g., ELAL) is given by the coordinate velocity of that site, and that the appropriate error is the coordinate velocity error. Remaining stations in the transect have the lower errors appropriate to the baseline solution, adjusted as described above. Since the two faults are not parallel, we used the rate component relative to the strike of the Agua Blanca fault for the sites with relative velocity data, and used the component of motion parallel to plate motion, essentially parallel to the San Miguel-Vallecitos fault, for the remaining sites. The extent to which this procedure may bias the fault slip rate estimates is assessed in the next section, where we account for geometric effects with a three-dimensional block model.

[28] Fault slip rate uncertainties for the multiple parallel fault models are determined using the  $F$  test to estimate the  $\chi^2$  misfit value corresponding to the appropriate confidence interval:  $\chi_{95\%}^2 = \chi_{best}^2 [1 + (\frac{\nu_1}{\nu_2 - \nu_1})F]$ , where  $\chi_{best}^2$  is the best fit  $\chi^2$ ,  $\nu_1$  is the number of adjusted parameters (generally 2 or 3),  $\nu_2$  is the number of data (12–15), and  $F$  is the  $F$  ratio statistic computed at  $F_{\nu_1, \nu_2}$ . We term this the formal error of the rate estimate. In general these formal errors are smaller than the differences in rate estimates based on different rheological assumptions, as described below. For comparison we also generated modified data sets by omitting a single data point, substituting (double counting) the remaining rate data in succession to keep the total number of data constant, and evaluating a new best fit model (since the data set is small it is not feasible to eliminate more than 1 datum and still obtain representative solutions). In effect we eliminate one data point and successively increase the weight of the remaining data. This generates a total of 132 modified data sets (12 possible omissions times 11 substitutions), and 132 fault slip rate estimates, from which 95% confidence intervals can be estimated. On plots of contoured  $\chi^2$  misfit for fault slip rate estimates (Figures 6 and 9) we also plot the rate estimates from the 132 modified data sets; the two generate very similar patterns. The corresponding error estimates generally agree within 0.5 mm yr<sup>-1</sup>, with the  $\chi^2$  estimate typically larger.

[29] The best fitting rates for the Agua Blanca and San Miguel-Vallecitos faults are 2.9 ± 1.3 and 3.8 ± 1.1 mm yr<sup>-1</sup> respectively for the two-fault, elastic half-space model. For the Agua Blanca fault this is 0.2 mm yr<sup>-1</sup> slower compared to single-fault model, reflecting the strain effect of the second fault. In this example the difference is small, however several factors may influence this, especially the distance between the two faults. As noted in other studies [e.g., Bennett *et al.*, 1997; Dixon *et al.*, 1998] the overall slip rate across two adjacent faults (in this case, 6.7 ± 0.2 mm yr<sup>-1</sup>) is better constrained than the individual slip rates.

[30] The estimated rates may be influenced by the errors assigned to the individual data. In our case, the slip rate

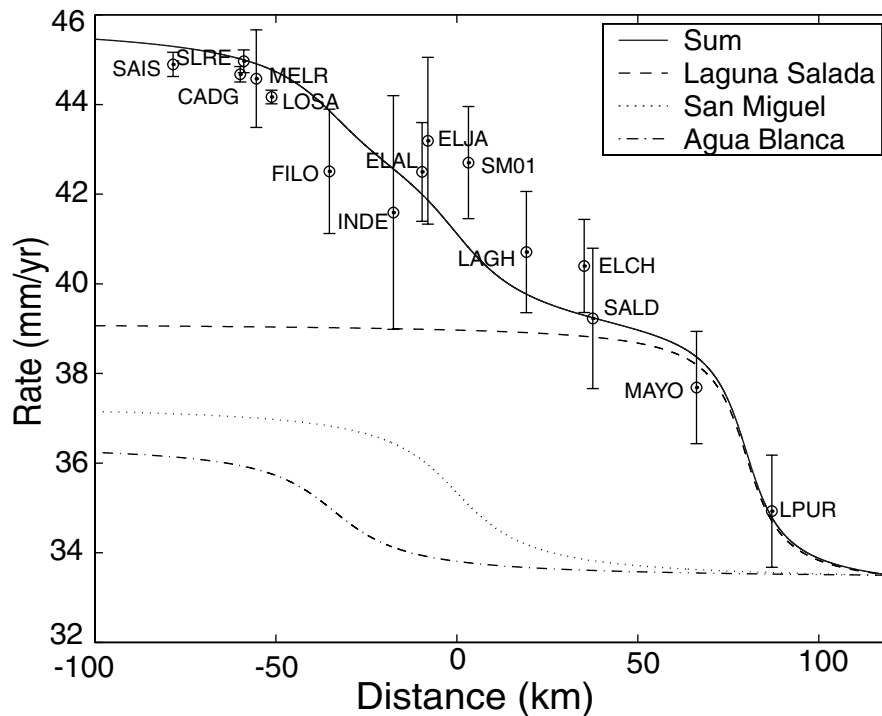


**Figure 5.** Velocity data and best fit elastic half space model for 3 parallel faults and 15 data, including three data (LPUR, MAYO, SMO1) from *Bennett et al.* [1996]. Rate estimates for Agua Blanca and San Miguel-Vallecitos faults are adjusted, rate for Laguna Salada fault is fixed at  $6 \text{ mm yr}^{-1}$ .

estimate for the Agua Blanca fault is influenced by the errors assigned to the relative position data (recall that we lack a rigorous, independent error model for these data). Reducing the uncertainties for the four relative position data by 50% increases the estimated slip rate for the Agua Blanca fault to  $3.5 \text{ mm yr}^{-1}$  and reduces the rate for the San Miguel-Vallecitos fault to  $3.3 \text{ mm yr}^{-1}$ . Increasing the uncertainties by 50% changes rates in the opposite sense, to  $2.7 \text{ mm yr}^{-1}$  and  $4.0 \text{ mm yr}^{-1}$  respectively.

[31] Figures 5 and 6 illustrate the effects of the Laguna Salada fault on the slip rate estimates (three-fault model). Here we treat the slip rate ( $6 \text{ mm yr}^{-1}$ ) and locking depth (7.5 km) for the Laguna Salada fault as fixed parameters [Bennett et al., 1996]. In addition, we can include three data points from *Bennett et al.* [1996], adjusted to a common reference frame as described previously, obtaining  $2.3 \pm 1.1 \text{ mm yr}^{-1}$  (Agua Blanca) and  $4.3 \pm 1.0 \text{ mm yr}^{-1}$  (San Miguel-Vallecitos). Without the three additional data, we obtain  $3.1 \text{ mm yr}^{-1}$  (Agua Blanca) and  $3.5 \text{ mm yr}^{-1}$  (San Miguel-Vallecitos). In either case the effect of the Laguna Salada fault makes less than  $1 \text{ mm yr}^{-1}$  difference to the slip rate estimates for the other two faults, reflecting the shallow locking depth of this fault, which limits strain effects to a relatively narrow zone. Including the Cerro Prieta fault also has only a small effect. Again, the sum of the Agua Blanca and San Miguel-Vallecitos slip rate estimates ( $6.6 \pm 0.2 \text{ mm yr}^{-1}$  with or without the additional data) is better constrained than the individual fault slip rates (Figure 6).

## 5.2. Block Model

[32] The Agua Blanca and San Miguel-Vallecitos faults are not parallel, differing in trend by up to  $25^\circ$ . Also, neither

fault is particularly straight or continuous, with discontinuous, occasionally en-echelon segments (Figure 1). To what extent do these geometric effects bias fault slip rate estimates when we assume straight, infinitely long, parallel faults, as in the analytical models described above?

[33] *Bennett et al.* [1996, 1997] describe an elastic half-space block model that accounts for these geometric effects to first order, and we follow essentially the same approach here. Briefly, we adopt a model consisting of discrete crustal elastic blocks in contact along planar boundaries [Matsu'ura et al., 1986], and use the formal inversion approach developed by *Bennett et al.* [1996]. Site velocities are referenced to the network centroid rather than stable North America, minimizing the dependence of results on possible reference frame biases. The block model comprises 3 blocks joined along 3 planar surfaces, with block boundaries coinciding with major fault zones spanned by the data (Figure 7). Block motion is represented as a simple translation rather than a rigid body rotation about an Euler pole because the block size is small compared to the Earth's radius, i.e., curvature across the study area is negligible. Neighboring blocks are assumed to be welded from the surface to a locking depth of 15 km. Relative motion between neighboring blocks induces elastic strain in the vicinity of the welded part of their common boundary. This is a "side-driven" model; we assume there is no strain associated with tractions below the welded parts of the block boundaries or along the bases of the blocks. With these assumptions, the geodetically observed velocity field within each block is modeled as the sum of a horizontal rigid body translation and spatially variable strain within the block. For simplicity we use only the coordinate velocity data listed in Tables 1 and 2.

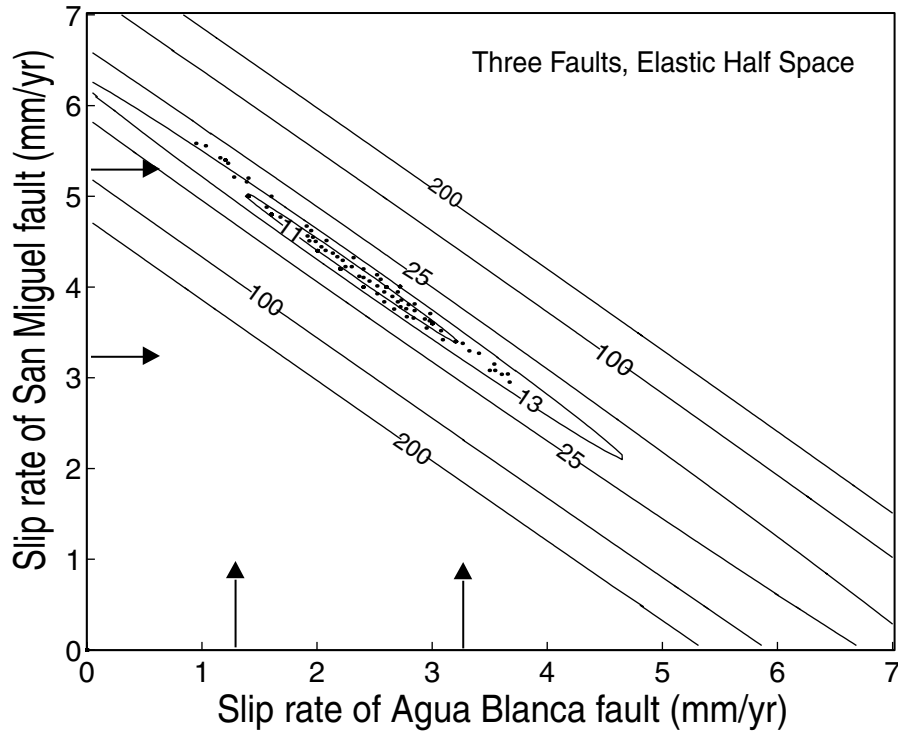


**Figure 6.** Contoured values of  $\chi^2$  misfit as a function of slip rate for the Agua Blanca and San Miguel-Vallecitos faults, for the elastic half space, 3 parallel fault model (Table 4; Figure 5). Dots show best fit models for various modified data sets (see text), and arrows bound 95% of these solutions.  $\chi^2 = 16$  marks approximate 95% confidence limit from the  $F$ -ratio statistic (see text).

[34] We identify the three-dimensional slip-rate vector associated with each model fault with the vector difference between the adjacent horizontal rigid block motions resolved onto the model fault planes. This parameterization differs somewhat from that of *Matsu'ura et al.* [1986] who modeled the slip rates as independent of the relative block motions, and from *Bennett et al.* [1996] in that block motions are not constrained by the orientations of the model faults, i.e., fault-normal motions are allowed. Rather, fault slip rates are inferred from the relative block motions, as derived from the geodetic observations. For the scenario in which all crustal strain is recovered seismically, we expect the fault slip rate estimates to match paleoseismological estimates assuming model rheology is realistic.

[35] The 3 slip-rate vectors of our model are determined by the 3 2-vectors describing horizontal block motions. We denote these block motions as a single model vector  $\mathbf{m}$ . The site velocity estimates are used to infer the  $\mathbf{M} = 6$  elements of the vector  $\mathbf{m}$ . To relate slip rates with block motions, we first define a slip-rate vector  $\mathbf{s}$ :

$$\mathbf{s} = \begin{pmatrix} s_1 \\ s_2 \\ s_3 \end{pmatrix} \quad (3)$$

where  $s_i$  is the slip-rate vector associated with the  $i$ th fault of our model. The vector  $\mathbf{s}$  has 9 components since each  $s_i$  is a three-dimensional vector. The relationship between  $\mathbf{s}$  and the model parameter vector  $\mathbf{m}$  is given by  $\mathbf{s} = \mathbf{F}\mathbf{m}$  where  $\mathbf{F}$  is a  $9 \times 6$  “fault geometry” matrix which maps horizontal

block motions into block motion differences resolved onto the block boundaries. The components of  $\mathbf{F}$  depend on the strike and dip of the fault plane. For vertical strike-slip faults, the dip-slip components of the slip-rate vectors are zero.

[36] To calculate the elastic strain at points on the Earth's surface associated with locked parts of faults, we use *Okada's* [1985] expressions for the response of rectangular dislocations in an elastic half-space, summing over the three-fault segments of the model. The formulae are invoked after transforming the station coordinates to a local Cartesian system. Because strain attenuates rapidly away from the near-surface locked parts of the faults, errors due to the local Cartesian approximation are negligible.

[37] We show results that respectively include or exclude station SFAI (Table 5). This site, not used in the “transect” approach described in section 5.1 (it is too far from the transect line) has a higher velocity compared to nearby sites that are a similar distance from the block boundary (SALD, ELCH), either due to data noise or due to along-strike differences in strain partitioning across the region (recall that the plate boundary zone is narrower for a plate motion-normal transect through SFAI compared to, for example, through CICE (e.g., Figure 1). Inclusion of SFAI's site velocity in the block model has the effect of decreasing the total velocity gradient across the Agua Blanca and San Miguel-Vallecitos faults, thus lowering their combined slip rates. Results with and without SFAI illustrate the sensitivity of our slip rate estimates to some individual site velocities for a relatively sparse data set such as ours. We

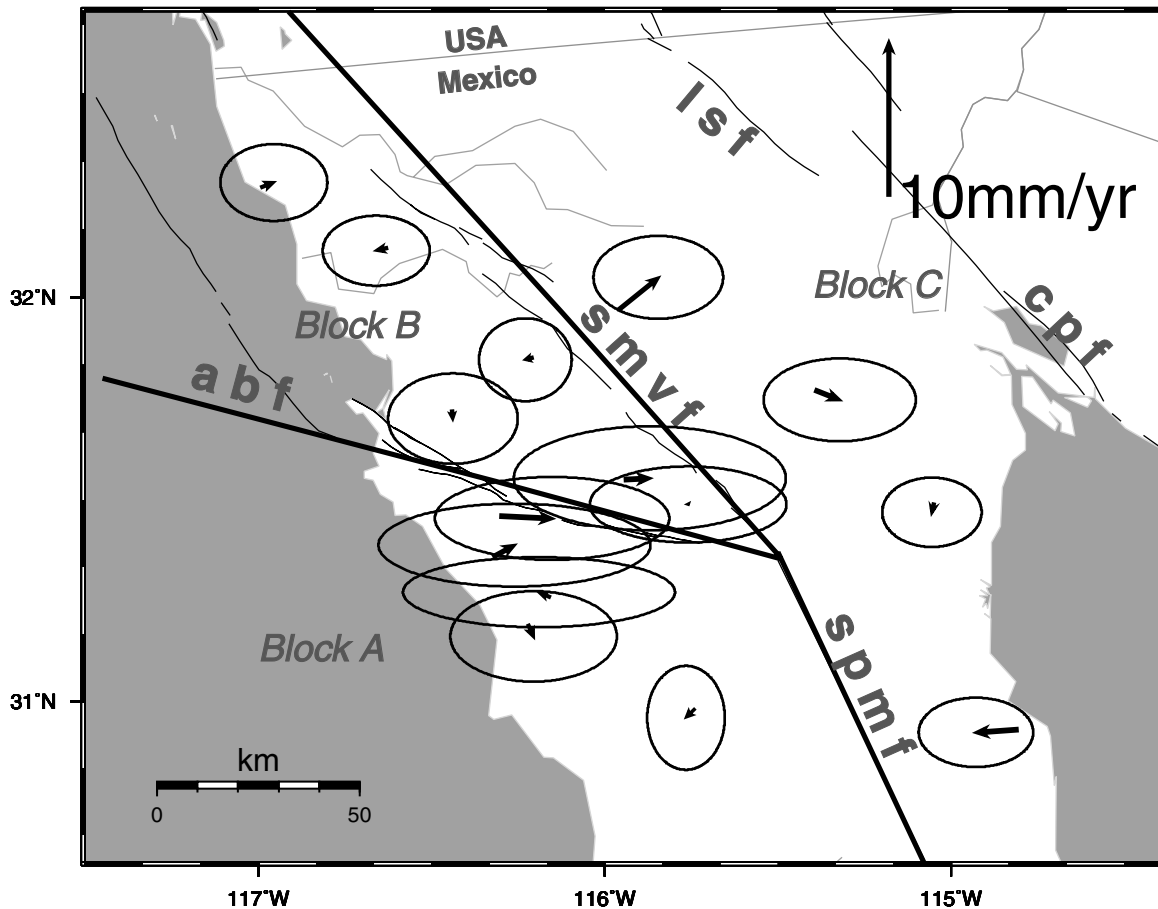


**Figure 7.** Velocity residuals from best fit three-dimensional block model, assuming elastic half space rheology. Block boundary approximations to major faults are shown as heavy straight lines. abf is Agua Blanca fault, smvf is San Miguel-Vallecitos fault, lsf is Laguna Salada fault, cpf is Cerro Prieto fault.

leave to a future study the effects of varying block size and fault geometry to better represent possible along-strike differences in the plate boundary zone. Here we take the result excluding SFAI as the best estimate, as it results in reduced misfit (Table 5). Despite significant differences in site distribution, the slip rate estimates for the Agua Blanca and San Miguel-Vallecitos faults are equivalent within uncertainties to the results of *Bennett et al.* [1996].

[38] The model that excludes SFAI is most comparable to the simple parallel-fault models described in the previous section; the predictions of the two models agree closely (Tables 4 and 5). Even the block model result that includes SFAI agrees with the parallel fault model within one standard error. Surprisingly, in spite of the oblique nature of the Agua Blanca fault, estimated fault-normal motion is small ( $0.5 \pm 0.9 \text{ mm yr}^{-1}$ ), insignificantly different from zero, and not significantly different from the fault-normal component for the San Miguel-Vallecitos fault.

[39] The San Pedro Martir fault (Figure 1) has a classic normal fault geometry, with a 3000 m high escarpment and a curvilinear trace with at least three scoop-shaped segments [Brown, 1978]. The Sierra San Felipe immediately to the east forms a sequence of west-dipping blocks in the hanging wall, consistent with normal motion on a listric, east-dipping normal fault. The fault has resolved normal motion in the correct sense only for the solution that excludes SFAI,

another indication that this data point may be spurious. The estimated horizontal extension rate ( $2.8 \pm 1.4 \text{ mm yr}^{-1}$  in the solution that excludes SFAI) is nevertheless smaller than the strike-slip component ( $5.3 \pm 1.2 \text{ mm yr}^{-1}$ ; Table 5). This latter rate is essentially identical to that obtained by *Bennett et al.* [1996] with an independent data set. The exposed trace of the San Pedro Martir fault suggests that it accom-

**Table 5.** Slip Rate Estimates for Three-Dimensional Elastic Half-Space Block Models

	AB, $\text{mm yr}^{-1}$	SMV, $\text{mm yr}^{-1}$	SPM, $\text{mm yr}^{-1}$	$\chi^2$	$\chi^2_\nu$
<i>All Data</i>					
Include SFAI					
Parallel	$2.3 \pm 1.6$	$2.4 \pm 1.5$	$4.5 \pm 1.1$	21.4	0.97
Perpendicular	$0.6 \pm 0.9$	$0.8 \pm 1.0$	$1.3 \pm 1.3$		
Exclude SFAI					
Parallel	$2.2 \pm 1.6$	$3.7 \pm 1.7$	$5.3 \pm 1.2$	15.6	0.71
Perpendicular	$0.5 \pm 0.9$	$-0.3 \pm 1.1$	$-2.8 \pm 1.4$		
<i>Bennett et al. [1996]</i>					
Parallel	$4 \pm 3$	$3 \pm 3$	$5 \pm 3$		
Perpendicular	$2 \pm 2$	—	$-5 \pm 3$		

AB is Agua Blanca fault, SMV is San Miguel-Vallecitos fault, SPM is San Pedro Martir fault. Positive perpendicular value indicates convergence, negative motion indicates extension.

modates mainly dip-slip motion, and the structures accommodating strike-slip motion are not clear (the existing GPS network is too coarse to delineate which faults are active). *Dokka and Meriam* [1982] and *Suarez-Vidal et al.* [1991] describe the nearby Valle de San Felipe fault, striking parallel to the San Pedro Martir fault and located 5–15 km to the east of its surface trace. *Miller et al.* [1991] suggest that these two faults constitute a paired normal-strike-slip fault system, with oblique extension at depth partitioned onto strike-slip and normal components at the surface. However, geomorphic evidence for dextral slip on the Valle de San Felipe fault is limited, and shear may be distributed over a broader area. *Lewis and Stock* [1998] document Pliocene to Recent oblique divergence (extension plus dextral shear) in the Sierra San Fermin, about 25 km east of the surface trace of the Valle de San Felipe fault, near the current coast line.

[40] Since the three-dimensional block model explicitly accounts for geometric effects, we take its results (Table 5) as the best estimate for the various fault slip rate estimates assuming elastic half-space rheology. The good agreement between the block model and parallel fault model is nevertheless an important result, because it suggests that simple parallel fault models are a useful approximation in regions dominated by strike-slip faulting, in cases where data quality may not warrant more sophisticated block models. This result, combined with the relatively small rates of fault-normal motion estimated for the Agua Blanca and San Miguel-Vallecitos faults, is exploited in the next section, where we address earthquake cycle effects with analytical parallel-fault models that incorporate rheological layering. Note also that three different reference frame definitions (single reference station; stable North America; network centroid) result in statistically insignificant differences to the fault slip rate estimates using the elastic half-space approximation.

### 5.3. Viscoelastic Coupling Model

[41] Elastic half-space fault models fit our geodetic data quite well, as demonstrated in the previous sections. Nevertheless, other data are not consistent with this model. For example, seismic observations in northern Baja California show that earthquakes are restricted to depths above about 20 km [*Frez and Frias-Camacho*, 1998; *Frez et al.*, 2000]. More than two thirds of the events reported by *Frez et al.* [2000] for a region around the San Miguel-Vallecitos fault are shallower than 15 km. The deeper crust and upper mantle here and in many other regions are presumably too weak to sustain significant shear stress, deforming to relieve these stresses rather than storing them as elastic strain to be released in future earthquakes. Layered coupling models are probably more realistic, and include a strong elastic layer (upper crust) over one or more weak viscous or viscoelastic layers or a half-space, corresponding to the warmer, more ductile lower crust and upper mantle [*Nur and Mavko*, 1974; *Savage and Prescott*, 1978; *Cohen*, 1982; *Thatcher*, 1983; *Li and Rice*, 1987; *Rydelek and Sacks*, 1990; *Pollitz and Sacks*, 1992, 1994; *Pollitz*, 1997; *Pollitz et al.*, 2000]. The boundary between the strong upper crust and weaker layers below represents the lower limit of brittle faulting and the maximum depth of crustal earthquakes, typically 10–20 km in strike-slip zones. *Savage and Lisowski* [1998] present

one such model, with an elastic layer overlying a Maxwell viscoelastic half-space, with surface velocity  $v$  given by:

$$v = \sum_{n=1}^{\infty} (b_n/\pi) [\arctan\{x/((2n-1)H)\} - \arctan\{x/((2n+1)H)\}] \quad (4a)$$

$$b_{n+1} = b_1 (\tau_0^n/n!) \sum_{k=0}^n n!/[k!(n-k)!] a_{k+1} (t/T)^{n-k} \quad (4b)$$

where  $x$  is the horizontal distance from the fault,  $H$  is the elastic layer thickness,  $t$  is the time since the last earthquake, and  $T$  is the earthquake recurrence interval. Expressions for  $a_k$  are given in the appendix to *Savage and Lisowski*. Following *Savage and Lisowski* [1998], we set  $H$  to 12 km for most models. The time constant  $\tau_0$  is related to the earthquake recurrence interval and relaxation time for the half-space,  $\tau_0 = \mu T/2\eta$ , where  $\mu$  is the rigidity of the half-space, set here to  $3 \times 10^{10}$  Pa, and  $\eta$  is the viscosity, for most models set to  $3 \times 10^{19}$  Pa s [*Kenner and Segall*, 2000].

[42] This version of a viscoelastic coupling model, when implemented for multiple faults, assumes parallel faults. Since the three-dimensional elastic block model and the simple parallel-fault elastic model give similar results for the fault-parallel (strike-slip) component, the parallel fault approximation is probably adequate.

[43] For the San Miguel-Vallecitos fault, the last significant earthquake was in 1956 when three events, with moment magnitudes of 6.7, 6.3 and 6.2, occurred on the fault within about one week [*Doser*, 1992]. Right lateral surface rupture of about 80 cm was observed over a 20 km distance [*Shor and Roberts*, 1958], but aftershocks suggested an active fault trace about 100 km long [*Reyes et al.*, 1975; *Johnson et al.*, 1976]. *Doser* [1992] estimates an average of 1.3 meters of slip at depth for the largest (M 6.7) event). If the slip rate on this fault is  $3 \text{ mm yr}^{-1}$  [*Bennett et al.*, 1996], it would take 430 years to accumulate 1.3 meters of slip. *Hirabayashi et al.* [1996] report evidence for a previous earthquake on the fault approximately 500–700 years ago. We tested models with earthquake recurrence intervals of 250, 500 and 750 years.

[44] For the Agua Blanca fault, the recurrence interval and date of last earthquake are not well known. The oldest buildings in the nearby city of Ensenada are about 100 years old; they include unreinforced masonry structures that are in good condition. Spanish missions were established in the area approximately 200 years ago and there are no reports of large earthquakes in the region from that time, nor any obvious ground breaks that might have occurred in the last 200 years. Thus the recurrence time is likely greater than 200 years, and the time of the last earthquake is likely prior to 1800 AD, assuming periodic earthquakes. *Rockwell et al.* [1993] determine the recurrence interval for the Agua Blanca fault in several ways. Using a model of fault segment length and characteristic seismic offset, they estimate 90–250 years. Using a dated offset feature and assuming that this offset accumulated in a regular series of earthquakes, they estimate 100–375 years. Trenching studies suggest that the last rupture of the Punta Banda segment may have occurred as recently as 200–300 years ago. We

**Table 6.** Slip Rate Estimates, Coupling Models

Recurrence Interval Years		Slip Rate, mm yr <sup>-1</sup>		$\chi^2$	$\chi^2_\nu$
AB	SMV	AB	SMV		
<i>Slip Rate Estimates for Multiple-Fault Viscoelastic Coupling Model, With Date of Last AB Event = 1800 AD</i>					
200	250	6.2 ± 1.0	1.2 ± 0.6	4.4	0.44
400	250	5.2 ± 1.2	1.7 ± 0.7	5.6	0.56
200	500	6.4 ± 1.0	1.0 ± 0.6	4.7	0.47
400	500	6.3 ± 1.3	0.8 ± 0.8	6.7	0.67
200	750	7.0 ± 1.0	0.6 ± 0.6	4.6	0.46
400	750	6.6 ± 1.4	0.5 ± 0.8	7.1	0.71
<i>Slip Rate Estimates for Multiple-Fault Viscoelastic Coupling Model, With Date of Last AB Event = 1700 AD</i>					
300	250	6.3 ± 1.2	1.6 ± 0.7	5.5	0.55
300	500	6.8 ± 1.2	1.0 ± 0.7	5.5	0.55
400	250	6.4 ± 1.1	1.1 ± 0.7	4.9	0.49
400	500	6.7 ± 1.1	1.0 ± 0.7	4.9	0.49

AB is Agua Blanca fault, SMV is San Miguel-Vallecitos fault.

tested models for the Agua Blanca fault with recurrence intervals between 200 and 400 years, and with the date of last event fixed to either 1800 AD or 1700 AD, adjusting the slip rates for best fit in each case. With these constraints, we have two adjustable parameters (two slip rates) for a simple two-fault model, constrained by 12 GPS rate data.

[45] Table 6 shows the best fit fault slip rate estimates for several two fault coupling models with differing assumptions. The data and best fit model are shown in Figure 8, with model parameters listed in the figure caption. Figure 9 shows misfit versus slip rate on both faults. The summed

slip rate for the two faults in the best fit model is  $7.4 \pm 0.2$  mm yr<sup>-1</sup>. This model predicts a slip rate for the Agua Blanca fault ( $6.2 \pm 1.0$  mm yr<sup>-1</sup>) that is considerably faster than any of the elastic half-space models (2.2–3.1 mm yr<sup>-1</sup>). A viscoelastic coupling model that uses recurrence intervals for the two faults in the middle of the plausible ranges described above and a date of 1750 AD for the last Agua Blanca event predicts slip rates of 6.8 mm yr<sup>-1</sup> and 0.9 mm yr<sup>-1</sup> respectively for the Agua Blanca and San Miguel-Vallecitos faults. Even the slowest viscoelastic coupling model rate ( $5.2 \pm 1.2$  mm yr<sup>-1</sup>) is faster than any of the elastic half-space model rates for the assumed viscosity ( $3 \times 10^{19}$  Pa s), and the best fit rate for the San Miguel-Vallecitos fault is slower than any of the elastic half-space model rates for all tested viscosities ( $1-5 \times 10^{19}$  Pa s).

[46] We explored the sensitivity of the data to the paleoseismic parameters. The data are not sensitive to recurrence interval, but do have some sensitivity to the date of the last event. Figure 10 plots  $\chi^2$  misfit versus date of the last earthquake, assuming recurrence intervals of 200 and 400 years. The best fitting dates are 1800 and 1840 AD for the two recurrence intervals. The uncertainty is asymmetric, and the acceptable range is between 1750 AD and 1875 AD, consistent with available geologic data [Rockwell *et al.*, 1993].

[47] Models with differing viscosity, from  $1-5 \times 10^{19}$  Pa s, can result in rates for the Agua Blanca fault up to a factor of two slower from those presented above, but the Agua Blanca fault is always significantly faster than the San Miguel-Vallecitos fault. We also ran models for three and four faults, incorporating the effect of the Laguna Salada and Cerro Prieta faults. Assuming a shallow locking depth

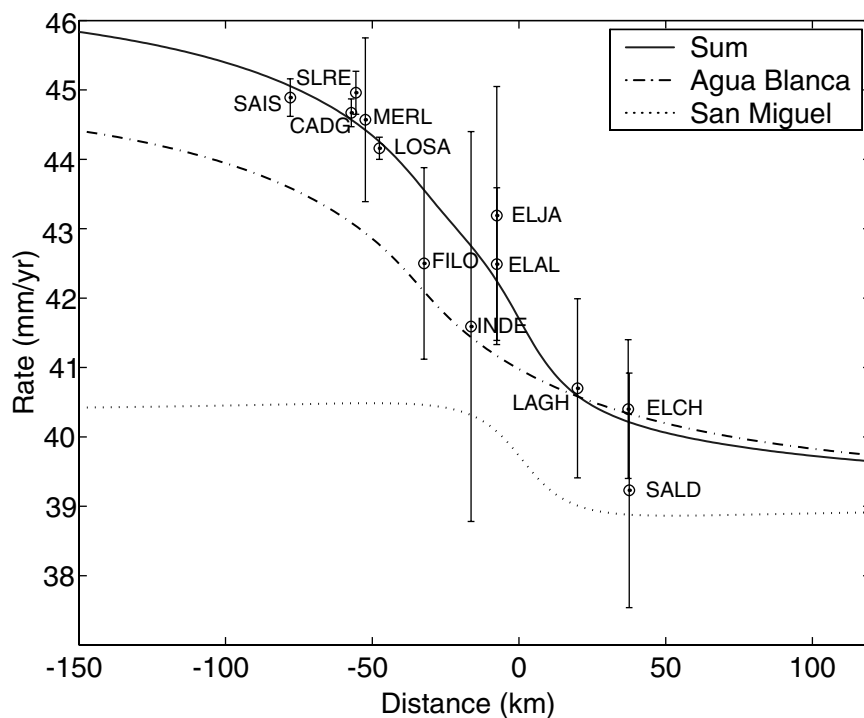


**Figure 8.** Velocity data and best fit viscoelastic coupling model for 2 parallel strike-slip faults, adjusting only the fault slip rates. Recurrence intervals for the Agua Blanca and San Miguel-Vallecitos faults are 200 and 250 years respectively, and date of last earthquake on the Agua Blanca fault is 1800 AD (Table 6a).

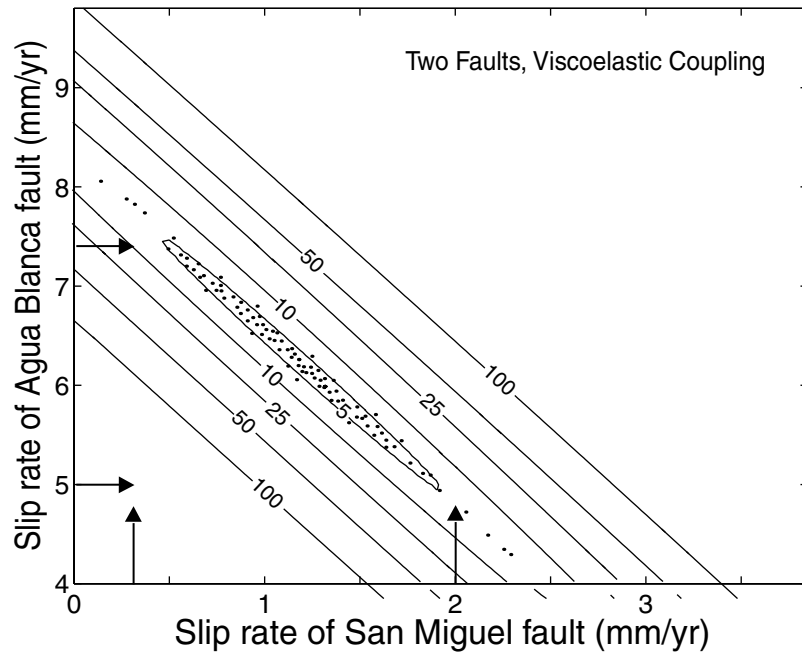


**Figure 9.** Similar to Figure 6, for viscoelastic coupling model.  $\chi^2 = 8$  marks approximate 95% confidence limit.

for these faults [Bennett *et al.*, 1996], there are negligible differences with results discussed above, e.g., no more than about  $1 \text{ mm yr}^{-1}$  difference in slip rate estimates, again with the Agua Blanca rate always faster than the San Miguel-Vallecitos rate. However, results are sensitive to locking depth, as well as assumptions about the earthquake cycle and half-space viscosity, and these deserve additional study. For example, using a 10 km locking depth for the Cerro Prieta fault and earthquake information from *Frez and Gonzalez* [1991] we obtain  $3.4 \text{ mm yr}^{-1}$  for the Agua Blanca fault and  $0.1 \text{ mm yr}^{-1}$  for the San Miguel-Vallecitos fault. Models that place essentially all slip on the Cerro Prieta and Laguna Salada faults fit the GPS data nearly as well, although these models are less consistent with other data. These results emphasize the importance of incorporating accurate geological (recurrence interval, date of last earthquake) and rheological constraints in our geodetic models, and suggest that additional work in these areas will be required before we can define accurate fault slip rates for this and perhaps other regions with GPS.

#### 5.4. Three-Dimensional Viscoelastic Model

[48] The kinematic models discussed so far allow us to estimate present-day fault slip rates (with some assumptions), but do not explain why certain faults appear to be more active than others. For example, why does the Agua Blanca fault apparently accommodate significant slip despite misalignment with plate motion? We have begun to address these issues with a series of finite element models using the code TECTON [Melosh and Raefsky, 1980]. The model is implemented in a fully three-dimensional form [Govers, 1993] and incorporates fault geometry, rheological layering and earthquake cycle effects. A comparison of the outputs of the finite element model and the analytical coupling model for a single vertical strike-slip fault and identical conditions is shown in Figure 11. Surface velocity

predictions are equivalent within model uncertainties, mainly limited by mesh size in the finite element model (to our knowledge this is the first published comparison of these two approaches).

[49] Three-dimensional model geometry for northern Baja California is shown in Figure 12. The rectangular model domain is rotated into the local plate motion orientation, extending 450 km in the direction perpendicular to plate motion and 180 km in the parallel direction. As with

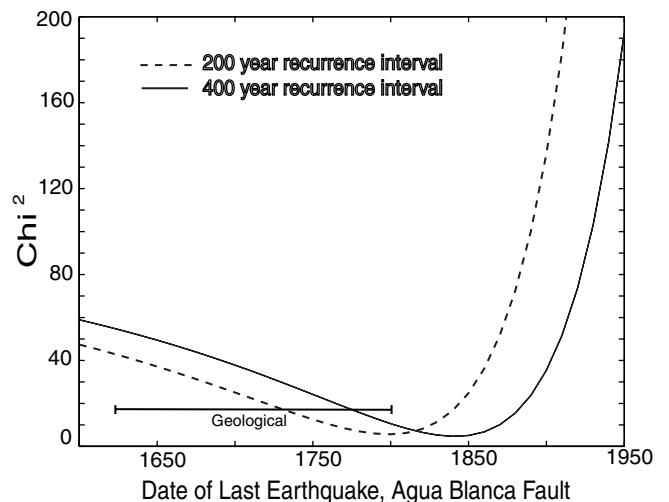


**Figure 10.**  $\chi^2$  misfit as a function of date of last earthquake on the Agua Blanca fault (viscoelastic coupling model) for two possible recurrence intervals, other parameters fixed to best fitting values. Note that dates earlier than 1800 AD are not defined for the 200 year recurrence interval given assumption of periodic earthquakes. Horizontal bar marks range of geological estimates (text).

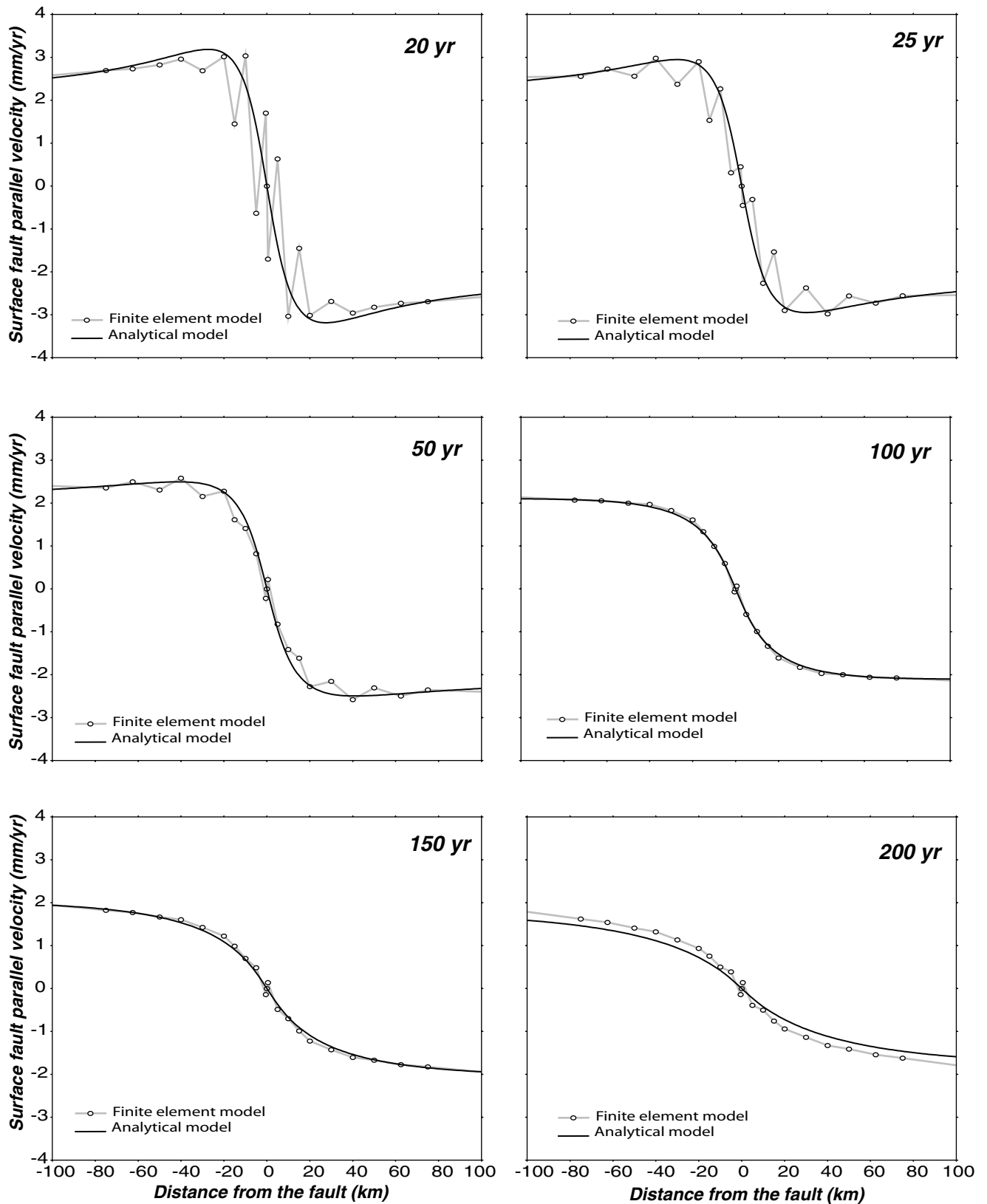


**Figure 11.** Comparison of predictions for analytical coupling model (equations 4a and 4b) locked throughout a 12 km thick elastic layer over a Maxwell viscoelastic half space, and finite element model with same rheology.

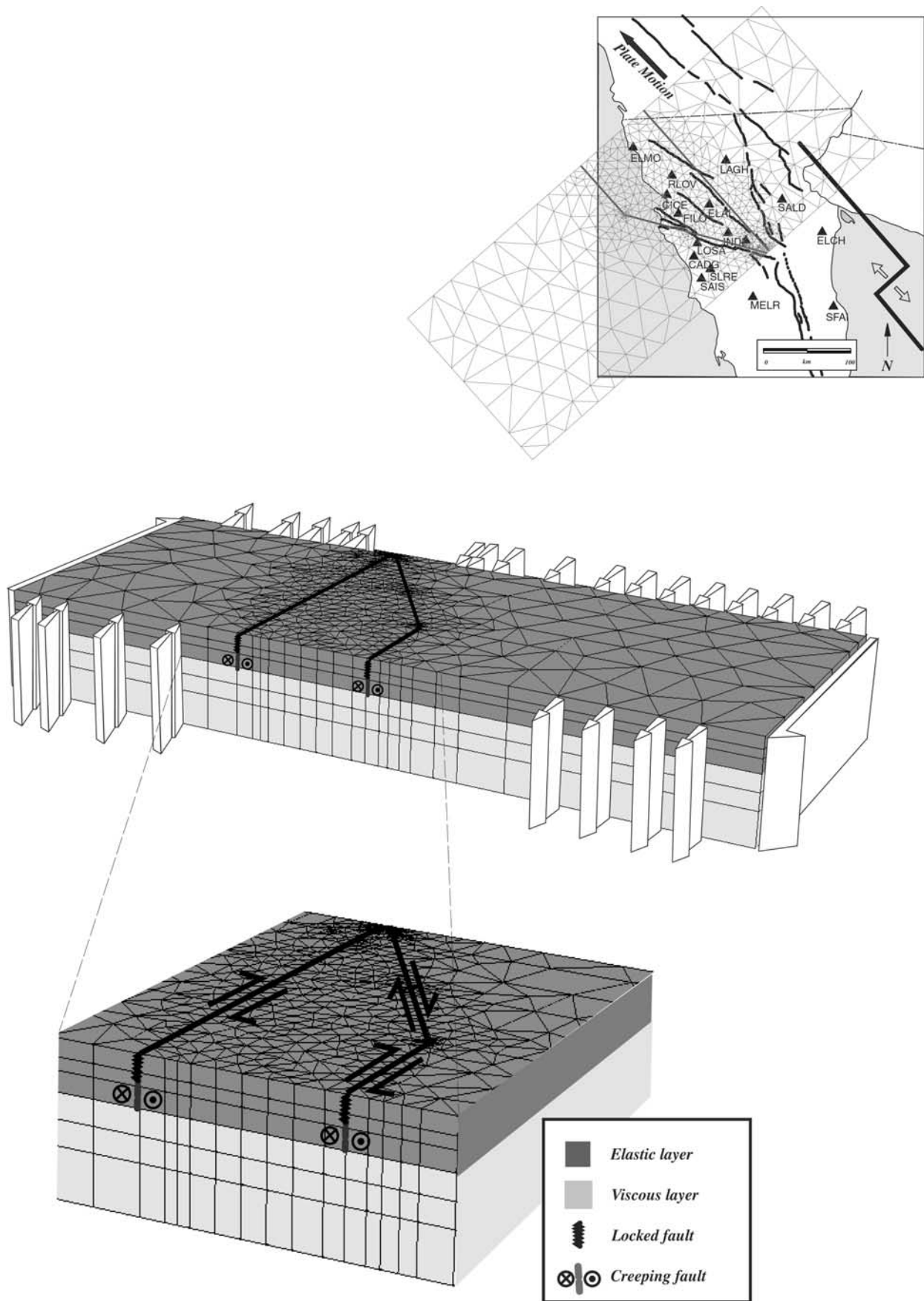


**Figure 12.** Finite element mesh, velocity boundary conditions, and rheological model used for the three-dimensional finite element model of northern Baja California.

the three-dimensional elastic half-space block model, we ignore Earth's curvature. The model domain is 60 km thick and includes the crust and most of the lithospheric mantle, represented by 4011 nodes and 6408 three-dimensional elements (triangular prisms). Rheology for most of the model runs is similar to the analytical coupling model, though perhaps more realistic, with three mechanical layers. While we retain an elastic upper crust overlying Maxwell viscoelastic material, faults are implemented differently, using a combination of split nodes in the upper 12 km to simulate fully locked faults [Melosh and Raefsky, 1981], and slippery nodes in a thin (8 km) elastic region beneath the upper layer to simulate creeping faults [Melosh and Williams, 1989]. Below 20 km the model is viscoelastic, with a viscosity of  $10^{19}$  Pa s. This is slightly lower than the value used for most of the analytical coupling models, but with a thicker elastic layer, response of the finite element model is very similar to the analytical model.

[50] Earthquakes in the finite element model are simulated by unlocking the upper locked portion of the fault for one time step, and displacing the crust on either side of the fault by the amount of coseismic slip (1.2–2.0 meters). Figure 12 shows fault locations within the elastic crust. We also tested a model in which the Agua Blanca fault was allowed to slip freely, simulating a low friction fault. Displacement rate boundary conditions ( $6.8 \text{ mm yr}^{-1}$ , intermediate between the range of values obtained in the kinematic models) were also specified on the sides of the model (large arrows in Figure 12). This differs from the kinematic models, where displacement rates were either specified for each of the fault segments and varied to obtain a good fit with the GPS data, or the data were inverted to find the minimum misfit model. Here we do not specify displacement rates on individual faults. Rather, we specify the integrated fault slip across the region as a velocity boundary condition (as measured by GPS, and largely independent of assumed rheology), and let the finite element model partition displacement according to assigned fault geometry, assumed rheology and earthquake cycle stage.

[51] Most models were run for the equivalent of  $\sim 370$  years. This allowed us to initialize the model for approximately 200 years, at which point a relatively steady state was reached, as expected for a viscosity of  $10^{19}$  Pa s. At 220 model years ( $\sim 150$  years BP), an Agua Blanca earthquake was prescribed (1.2 or 2.0 meters displacement), and at 320 model years ( $\sim 50$  years BP) a San Miguel-Vallecitos earthquake occurred (1.2 meter displacement). The present deformation field is most sensitive to the timing of the most recent earthquake. Whether an Agua Blanca event occurred 150 years BP or 250 years BP has little effect on the present-day deformation field, consistent with the sensitivity inferred from the two-dimensional analytical model.

[52] Figure 13 shows differences (residuals) between the prediction of our standard model (earthquakes of 1.2 meters on both the Agua Blanca and San Miguel-Vallecitos faults at the times given above) and the GPS observations. Misfit is within the two-dimensional 95% confidence ellipse at all stations, but there is a systematic pattern of misfit for sites just north of the Agua Blanca fault (ELMO, CICE, FILO, and INDE). Thus the actual velocity gradient across the Agua Blanca fault is higher than that predicted by the model

i.e., the fault slip rate is higher than predicted by the finite element model for the listed conditions (discussed below).

[53] Although we do not specify a slip rate on any of the faults in this model, we can estimate the long-term slip rate by analyzing the model velocities in the middle crust beneath the locked layer. For the model results in Figure 13 (i.e., with misfit north of the Agua Blanca fault), the modeled velocity partitions onto the two faults with approximately  $1.5 \text{ mm yr}^{-1}$  on the Agua Blanca fault and  $4.5 \text{ mm yr}^{-1}$  on the San Miguel-Vallecitos faults. This value changes continually throughout the earthquake cycle with short-term rates as high as  $3.2 \text{ mm yr}^{-1}$  on the Agua Blanca fault 30 years after the simulated earthquake. This behavior is consistent with the predictions of the two-dimensional analytical viscoelastic coupling model. The 1.5:4.5 partitioning of the velocity at present is similar to the partitioning in the model prior to any earthquakes (200 model years). Surface deformation patterns are not well fit without the earthquakes, particularly northeast of the San Miguel-Vallecitos fault system.

[54] Models in which Agua Blanca earthquakes are larger (2.0 meters instead of 1.2 meters) produced larger partitioning onto the Agua Blanca fault immediately after the earthquake but do not significantly improve the fit long after the event.

[55] Intuitively, it makes sense that the better-oriented San Miguel-Vallecitos fault will accommodate the majority of plate motion. However, the model misfits north of the Agua Blanca fault (Figure 13) imply that more slip must be partitioned onto this fault in order to match the data, qualitatively consistent with the predictions of the analytical coupling model. To evaluate the respective roles of fault geometry and fault friction, we ran models where the Agua Blanca fault was allowed to slip freely, simulating a low friction fault. In this case velocity partitions  $\sim 3.5 \text{ mm yr}^{-1}$  on the Agua Blanca fault and  $\sim 3 \text{ mm yr}^{-1}$  on the San Miguel-Vallecitos fault. This model fits the GPS data somewhat better, lending credence to the concept that there may be less net resistance to slip on the Agua Blanca fault compared to the San Miguel-Vallecitos fault, despite the former being misaligned with the plate motion direction.

## 6. Discussion

### 6.1. Impact of Rheological Model

[56] GPS or other high precision geodetic data are often used to estimate fault slip rates with a rheological model for the crust and upper mantle, relating measured site velocities at various distances from the fault to theoretical “far field” velocities that presumably relate to long-term geological slip rates. One conclusion from this study is that the rheological model used can have a significant impact on fault slip rate estimates. Assuming elastic half-space rheology, the San Miguel-Vallecitos fault ( $2.4\text{--}3.7 \text{ mm yr}^{-1}$ ) appears to be a major fault in the region, accommodating equivalent or somewhat greater motion than the Agua Blanca fault ( $2.2\text{--}3.1 \text{ mm yr}^{-1}$ ). In contrast, an analytical coupling model that incorporates the effects of viscoelastic lower crust/upper mantle and earthquake history suggests a very different picture, with the San Miguel-Vallecitos fault ( $1.2 \pm 0.6 \text{ mm yr}^{-1}$ ) slipping significantly slower than the Agua Blanca fault ( $6.2 \pm 1.0 \text{ mm yr}^{-1}$ ). The assumed

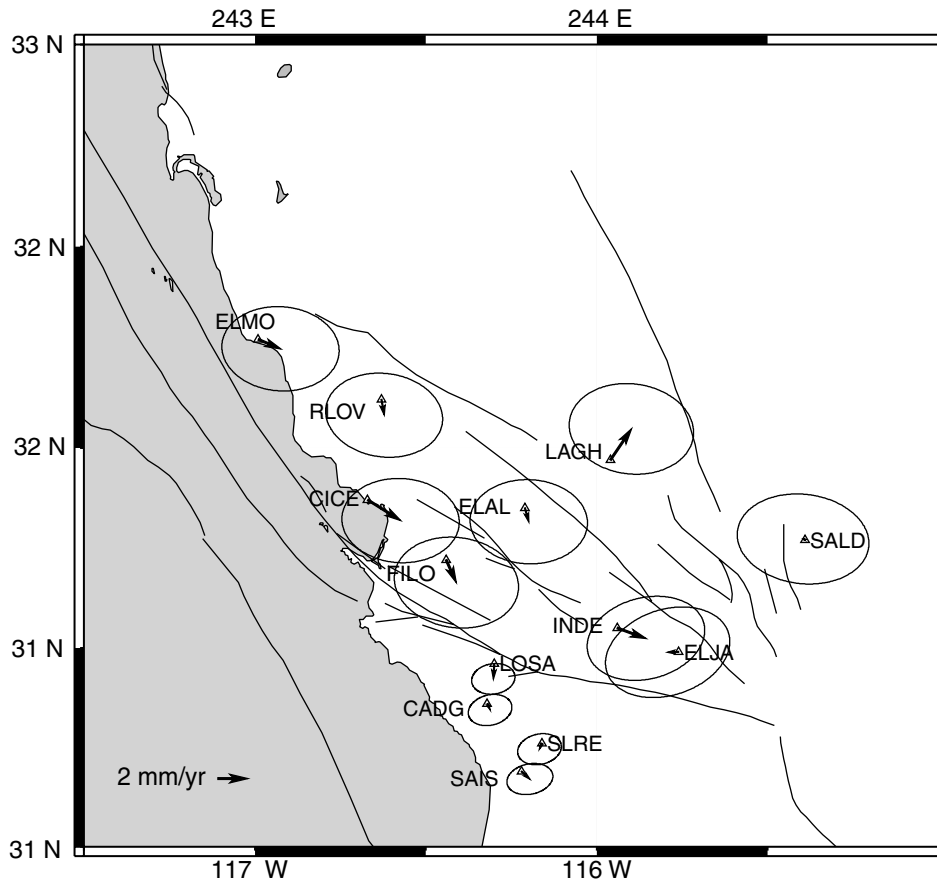


**Figure 13.** Residuals (observed velocity minus velocity predicted by the three-dimensional finite element model) and 95% confidence ellipses. Note systematic misfit at sites ELMO, CICE, FILO, and INDE, representing a low velocity “band” north of the Agua Blanca fault in the standard finite element model (equivalent properties for both faults).

viscosity for the lower crust/upper mantle can affect these estimates considerably, but for all tested analytic coupling models the Agua Blanca fault is considerably faster than the San Miguel-Vallecitos fault.

[57] *Hirabayashi et al.* [1996] report a maximum slip rate for the San Miguel-Vallecitos fault of  $0.55 \text{ mm yr}^{-1}$  by dating an offset Late Quaternary alluvial ridge with soil stratigraphic techniques, nearly equivalent to our coupling model estimate within one standard error, but much slower than any of the elastic half-space model results. Thus, predictions of the viscoelastic coupling model agree better with geological data for this fault than models assuming elastic half-space rheology.

[58] Geological rates for the Agua Blanca fault are less well defined, although available data are consistent with the fast rate interpretation suggested by the viscoelastic coupling model. *Suarez-Vidal et al.* [1991] report Quaternary fans offset up to 5 km along the Agua Blanca fault. Presuming a maximum age of 1.6 million years for these features (base of Quaternary) suggests a minimum slip rate of  $3 \text{ mm yr}^{-1}$  over this period. *Rockwell et al.* [1993] report a range of slip rate estimates for two segments of the Agua Blanca fault, ranging from a low of  $1.3 \text{ mm yr}^{-1}$  on one section of the Punta Banda Ridge segment to a high of  $10.6 \text{ mm yr}^{-1}$  on one segment within the Valle Agua Blanca. The Punta Banda Ridge segment lies at the west end of the on-

land exposure of the fault, where it splays into several strands (Figure 1). Measurements on this segment may not capture the full, integrated slip rate across the entire fault zone if motion is distributed on the various strands. We calculated the weighted mean and the weighted RMS scatter about the mean for the five best-determined slip rate estimates (range  $4.1\text{--}10.0 \text{ mm yr}^{-1}$ ) from the Valle Agua Blanca data of *Rockwell et al.* [1993], obtaining  $5.4 \pm 1.8 \text{ mm yr}^{-1}$ . We also recalculated the slip rates for the five sections under slightly different assumptions, dividing the best estimate of offset by the best estimate of the age of the offset feature, assuming symmetric uncertainties for both age and offset, and arbitrarily assigning an age uncertainty of  $\pm 10\%$  if no uncertainty was reported. This yields a weighted mean and RMS scatter of  $4.9 \pm 1.9 \text{ mm yr}^{-1}$ . Both approaches yield geological estimates that agree with the coupling model predictions the within one standard error.

[59] In summary, all of the tested elastic half-space models agree with each other within one standard error, regardless of which reference frame is used or whether fault geometry is accounted for. Models that incorporate viscoelastic rheology differ significantly from the predictions of these elastic half-space models. Geologic estimates for the Agua Blanca fault agree with all the geodetic models (both elastic and viscoelastic) within uncertainties, but agree

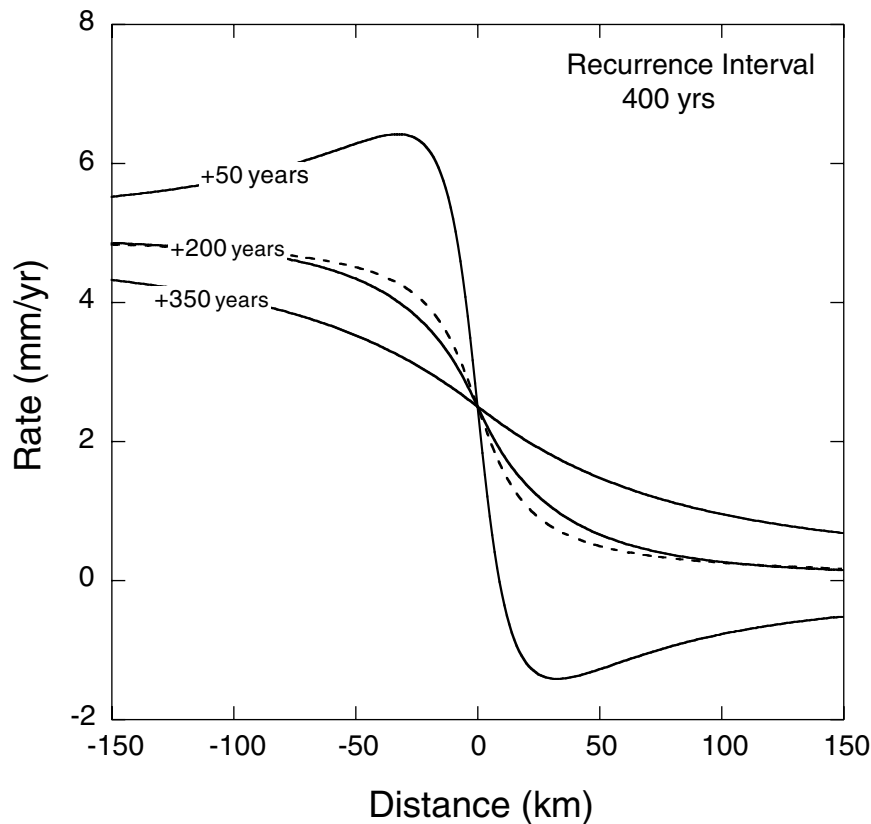


**Figure 14.** Calculated velocity profiles across a vertical strike-slip fault with a long-term slip rate of  $5 \text{ mm yr}^{-1}$ . Solid lines show predictions of the viscoelastic coupling model [Savage and Lisowski, 1998] for several times after the last earthquake (recurrence interval 400 years), assuming an elastic layer thickness of 12 km, rigidity of  $3 \times 10^{10} \text{ Pa}$ , and viscosity of  $3 \times 10^{19} \text{ Pa s}$ . Dotted line shows prediction of the simple elastic half space model [Savage and Burford, 1973] with a locking depth of 16 km.

better with the viscoelastic models. Geologic rate estimates for the San Miguel-Vallecitos fault agree only with the analytic viscoelastic models. Thus, of the various effects tested that might influence fault slip rate estimates from geodetic data, including parallel fault versus realistic geometry, reference frame, inclusion or exclusion of particular data, and data weighting, only the assumed rheology makes a significant difference. Models that incorporate viscoelastic behavior beneath an elastic upper crust agree better with geologic data, but are sensitive to the assumed rheology and earthquake cycle effects, emphasizing the importance of incorporating additional information.

[60] Why should the slip rates predicted by the different model rheologies differ so greatly, and why should the predictions of the coupling model agree better with geological data? Figure 8 shows the model velocity profiles for each fault. The profile for the San Miguel-Vallecitos fault has a steeper velocity gradient near the fault compared to the Agua Blanca fault, because the Agua Blanca fault is in a later stage of its earthquake cycle. Since the near-fault data strongly constrain the total slip rate (interpretation of far field data for the San Miguel-Vallecitos fault is complicated by the overlapping strain fields of adjacent faults), fitting each fault with an elastic half-space model with the same locking depth forces an overestimate of the slip rate for the San Miguel-Vallecitos fault, and a corresponding under-

estimate of the Agua Blanca fault. Thus the difference in estimated fault slip rates between the two rheological models mainly reflects the impact of the earthquake cycle on the observed velocity field near the faults.

[61] Figure 14 compares velocity profiles across a hypothetical strike-slip fault with a long-term slip rate of  $5 \text{ mm yr}^{-1}$ , for the viscoelastic coupling model at several times after an earthquake, and a simple elastic half-space model. In the middle of the earthquake cycle, the velocity profiles for the two models are essentially identical, differing everywhere by less than  $0.3 \text{ mm yr}^{-1}$ , below the noise limit for most displacement-type geodetic techniques. However, early and late in the cycle, the velocity profiles predicted by the two models differ significantly. Early in the cycle, viscous flow in the half-space, stimulated by coseismic slip, exerts a traction on the upper crust in the direction of coseismic offset, enhancing the surface velocity gradient near the fault. Geodetic measurements near the fault will capture this enhanced gradient, but unless far field measurements are also available (more than  $\sim 100$  kilometers from the fault, and in practice difficult to interpret in regions of multiple faults), application of the elastic half-space model may cause fault slip rates to be overestimated. Late in the cycle, the opposite situation obtains, and underestimation of the slip rate is possible if a standard (10–15 km) locking depth is assumed. In this case it is also possible to estimate

the correct long-term rate with an elastic half-space model if a deeper effective locking depth is used [Savage and Lisowski, 1998].

## 6.2. Evolution of the Trans-Peninsular Fault System and Geodetic Versus Geologic Rates

[62] The summed slip rate across the Agua Blanca and San Miguel-Vallecitos faults (range 4.7–7.9 mm yr<sup>-1</sup> for all multifault models tested, regardless of assumed rheology) is better constrained than the individual fault rates, and represents about 10%–15% of overall Pacific North America motion at this location. *Humphreys and Weldon* [1991] termed these faults the Trans-Peninsular Fault system, and emphasized the important kinematic role they play in allowing some deformation to bypass the restraining “big bend” in the San Andreas fault. The Trans-Peninsular fault system “feeds” slip across the northern Baja California peninsula, through the southern California borderland, and into the western Transverse Ranges, and in turn is “fed” by one or more transform faults in the Gulf of California. *Miller et al.* [1991], *Suarez-Vidal et al.* [1991], and others have suggested that the Agua Blanca and San Miguel-Vallecitos faults connect via the San Pedro Martir-Valle de San Felipe fault system (a paired normal-right lateral strike-slip fault system) to the Ballenas-Salsipuedes transform fault, a long transform fault in the Gulf of California connecting two short rift segments, the Guaymas and Delfin rifts [e.g., *Ness and Lyle*, 1991; see also *Humphreys and Weldon*, 1991, Figure 1]. Thus the Gulf transform fault does not cease activity at its intersection with the spreading center, as it should in a simple ridge-transform system. Instead, slip continues northwest past the spreading center at a reduced rate, forming a type of triple junction, separating two plates (Pacific, North America) and a deforming continental “sliver” block or microplate (northern Baja California and southern California, northeast of the Agua Blanca fault and southwest of the San Andreas fault). The Swan Island Fracture Zone in the Caribbean is another example, continuing east past its intersection with the Cayman Trough spreading center, through Jamaica (Plantain Garden fault zone) and Hispaniola (Enriquillo fault zone). The latter two faults form an important part of the Caribbean-North America plate boundary zone [Rosencrantz and Mann, 1991; Mann et al., 1995; Dixon et al., 1998]. In this case the triple junction at the southern end of the Cayman Trough lies at the boundary of the North American and Caribbean plates and the Gonave microplate. *Mann et al.* [1995] relate the development of this microplate to a restraining bend in the plate boundary zone, associated with collision between Hispaniola and the Bahama Platform. Common features among these strike-slip systems thus include a long transform fault intersecting a short spreading ridge segment, continued strike-slip motion past the ridge intersection at reduced rate, and possible development of these systems as a way to accommodate and bypass transpressional bends. The tectonics of such systems may evolve rapidly, hence geodetic rates for individual faults are not necessarily equivalent to geologic rates averaged over a few million years.

## 6.3. Friction Versus Misalignment

[63] The finite element model allows us to investigate why motion is accommodated on the misaligned Agua

Blanca fault. A model that assumes equivalent rheologic and frictional conditions on both faults systematically misfits the data, underpredicting the velocity gradient across the Agua Blanca fault. This may be a consequence of the rheologies and frictional behavior for the faults, assumed equal in our “standard” model. A better fit to the data is obtained for a model where resistance to slip on the Agua Blanca fault is lower compared to the San Miguel Vallecitos fault. This might reflect the longer period of activity (several million years) and/or larger offset (>15 km) of the Agua Blanca fault, compared to the San Miguel-Vallecitos fault, probably less than 500,000 years old, assuming a slip rate of 1 mm yr<sup>-1</sup> and a maximum offset of 500 meters. *Wesnowsky* [1988] observed that faults with larger cumulative offset are straighter, with longer segments and fewer “jogs” compared to small offset faults. The Agua Blanca and San Miguel-Vallecitos faults fit this pattern. Repeated faulting on the Agua Blanca fault may straighten out and lengthen short, en-echelon segments, reduce “asperities” (strong zones), and develop thick (low friction?) gouge zones in the upper, high strength frictional part of the crust [Scholz, 1990, chapter 3]. In contrast, the small-offset San Miguel-Vallecitos fault must crack new, intact crust, giving higher resistance to slip. Stress-drops for earthquakes on the San Miguel-Vallecitos fault tend to be higher for a given seismic moment than other earthquakes in the region [Thatcher, 1972; Doser, 1992]. Stress-drop is proportional to  $M_0/L^3$ , where  $M_0$  is seismic moment and  $L$  is source dimension, implying that San Miguel-Vallecitos earthquakes tend to be high stress-drop events on small fault patches.

[64] Low friction conditions facilitate motion on nonoptimally oriented fault planes [Ivins et al., 1990]. *Hill and Thatcher* [1992] suggest that lowering the effective friction coefficient of the upper crust by 20–25% can cause faults that are 20° misaligned with the optimum direction to slip preferentially. Misalignment of the Agua Blanca fault may therefore be compensated by lower frictional resistance to shear.

## 6.4. Seismic Hazard

[65] The Agua Blanca fault is seismically quiet at present. Our results suggest that this is not due to fault inactivity. Rather the fault is active, locked, and accumulating elastic strain, presumably to be released in a future earthquake. In addition, our results suggest that the Agua Blanca fault may be slipping at a faster long-term rate than generally assumed, and may be in a relatively late stage of its earthquake cycle. Assuming minimum and maximum times since the last earthquake of 200 and 400 years, and slip rates of 3 and 6 mm yr<sup>-1</sup>, implies 0.6 m–2.4 m slip accumulation. The minimum and maximum seismic moment,  $M_o$ , can be estimated from:

$$M_o = \mu \alpha D A \quad (5)$$

where  $\mu$  is the shear modulus ( $3 \times 10^{10}$  N/m<sup>2</sup>),  $\alpha$  is an empirical parameter indicating the efficiency of conversion of strain accumulation to actual earthquake energy, accounting for the possibility of aseismic release as well as seismic release on subsidiary faults at different times, (set here arbitrarily to 0.75, i.e., 75% of accumulated strain energy will be released in the next earthquake),  $D$  is the mean

displacement, and  $A$  is fault area, assumed to be 12 km depth multiplied by fault length. Geological maps of the Agua Blanca fault [Suarez-Vidal et al., 1991] suggest that a typical segment length at the surface is about 15 km. Assuming one or three of these segments ruptures at one time gives minimum and maximum estimates. Using empirical relations between seismic moment  $M_o$  and earthquake moment magnitude  $M$  ( $M = 2/3 \log M_o - 10.7$  in cgs units [Hanks and Kanamori, 1979]) we obtain  $M \sim 6.1-6.8$  for future Agua Blanca events.

[66] A second approach is to use empirical relations between earthquake magnitude and surface displacement in an earthquake [Wells and Coppersmith, 1994, Figure 10]. Assuming minimum and maximum average displacements of 0.6 and 2.4 meters accumulated at depth, and assuming that the maximum surface displacement reaches 75% of these values, then the expected Moment Magnitude of a future event would be  $M \sim 6.5-7.0$ .

[67] An approach that is independent of our GPS estimates of slip rate and date of the last earthquake uses empirical relations between earthquake magnitude and surface rupture length [Wells and Coppersmith, 1994, Figure 9] combined with the mapped extent of fault segments. Assuming minimum and maximum rupture lengths of one segment (15 km) and three segments (45 km), then the expected Moment Magnitude of a future event would be in the range  $M \sim 6.5-7.0$ .

## 7. Conclusions

1. GPS data acquired between 1993 and 1998 show a velocity gradient of about  $5 \text{ mm yr}^{-1}$  across the Agua Blanca and San Miguel Vallecitos faults in northern Baja California, Mexico, and suggest that the long-term summed slip rate across these two faults is  $4-8 \text{ mm yr}^{-1}$ .

2. We tested the sensitivity of fault slip rate estimates to rheological model, reference frame, inclusion or exclusion of individual data points, and other analytical choices. Slip rate estimates for individual faults are mainly sensitive to the assumed rheological model. Elastic half-space models predict roughly equivalent slip rates for the two faults, in the range  $2-4 \text{ mm yr}^{-1}$ . Models that account for the earthquake cycle and include a viscoelastic lower crust/upper mantle suggest that the Agua Blanca fault slips at a long-term rate of about  $6 \pm 1 \text{ mm yr}^{-1}$ , while the San Miguel-Vallecitos fault slips at about  $1 \pm 1 \text{ mm yr}^{-1}$ , in better agreement with geological data. The rates are sensitive to the assumed viscosity and earthquake cycle effects, and can vary by a factor of two for plausible values (e.g.,  $3-6 \text{ mm yr}^{-1}$  for the Agua Blanca fault). Determining accurate slip rates for these faults will require a better understanding of rheological structure for the region, better earthquake cycle information and a comprehensive velocity field spanning the entire plate boundary zone.

3. GPS data combined with a simple viscoelastic coupling model suggest that the last earthquake on the Agua Blanca fault occurred between 1750 AD and 1875 AD, consistent with geological data and placing this fault in the middle to late stage of its earthquake cycle.

4. Simple seismic hazard calculations suggest that the Agua Blanca fault is capable of an  $M = 6.1-7.0$  earthquake every few hundred years.

5. Preliminary finite element models can be interpreted to indicate that in spite of misalignment with plate motion, slip on the Agua Blanca fault is favored over the San Miguel-Vallecitos fault because the former has lower resistance to slip, perhaps related to its larger cumulative offset ( $>15 \text{ km}$ ) compared to the San Miguel-Vallecitos fault ( $<500 \text{ meters}$ ).

[68] **Acknowledgments.** The GPS observations were funded by grants from NASA's Solid Earth and Natural Hazards program and NSF EAR 9807673 to THD. KPF and RM were supported by NSF-EAR 97-25187. Installation of the continuous GPS site at CICESE was supported by NASA and CONACYT, with technical assistance from UNAVCO and JPL. This site is now operated by the Southern California Earthquake Center. We also thank personnel at UNAVCO and CICESE for assistance with the field observations. Most figures were prepared with GMT [Wessel and Smith, 1995]. Comments by Gene Humphreys and an anonymous reviewer greatly improved the manuscript.

## References

- Allan, C. R., L. Silver, and F. G. Stehli, Agua Blanca fault, a major transverse structure of northern Baja California, Mexico, *Geol. Soc. Am. Bull.*, **71**, 457-482, 1960.
- Atwater, T., Implications of plate tectonics for the Cenozoic evolution of western North America, *Geol. Soc. Am. Bull.*, **81**, 3513-3536, 1970.
- Atwater, T., Plate tectonic history of the northeast Pacific and western North America, in *Geology of North America, Vol. N, Eastern Pacific Ocean and Hawaii*, edited by E. L. Winterer, D. M. Hussong, and R. W. Decker, pp. 21-72, Geol. Soc. Am., Boulder, Colo., 1989.
- Bennett, R. A., W. Rodi, and R. E. Reilinger, Global Positioning System constraints on fault slip rates in southern California and northern Baja Mexico, *J. Geophys. Res.*, **101**, 21,943-21,960, 1996.
- Bennett, R. A., B. Wernicke, J. Davis, P. Elosgui, J. Snow, M. Abolins, M. House, G. Stirewalt, and D. Ferrill, Global Positioning System constraints on fault slip rates in the Death Valley region, California and Nevada, *Geophys. Res. Lett.*, **24**, 3073-3076, 1997.
- Brown, L. G., Recent fault scarps along the eastern escarpment of the Sierra San Pedro Martir, Baja California, M.S. thesis, 108 pp., San Diego State Univ., San Diego, Calif., 1978.
- Cohen, S. C., A multilayer model of time dependent deformation following an earthquake on a strike slip fault, *J. Geophys. Res.*, **87**, 5409-5421, 1982.
- DeMets, C., and T. H. Dixon, New kinematic models for Pacific North America motion from 3 Ma to present: Evidence for steady motion and biases in the NUVEL-1A model, *Geophys. Res. Lett.*, **26**, 1921-1924, 1999.
- Dixon, T. H., S. Robaudo, J. Lee, and M. C. Reheis, Constraints on present-day Basin and Range deformation from space geodesy, *Tectonics*, **14**, 755-772, 1995.
- Dixon, T. H., A. Mao, and S. Stein, How rigid is the North American plate?, *Geophys. Res. Lett.*, **23**, 3035-3038, 1996.
- Dixon, T. H., A. Mao, M. Bursik, M. Heflin, J. Langbein, R. Stein, and F. Webb, Continuous monitoring of surface deformation at Long Valley Caldera with GPS, *J. Geophys. Res.*, **102**, 12,017-12,034, 1997.
- Dixon, T. H., F. Farina, C. DeMets, P. Jansma, P. Mann, and E. Calais, Relative motion between the Caribbean and North American plates based on a decade of GPS observations, *J. Geophys. Res.*, **103**, 15,157-15,182, 1998.
- Dixon, T. H., M. Miller, F. Farina, H. Wang, and D. Johnson, Present-day motion of the Sierra Nevada block, and some tectonic implications for the Basin and Range province, North American Cordillera, *Tectonics*, **19**, 1-24, 2000.
- Dokka, R. K., and R. H. Merriam, Late Cenozoic extension of northeastern Baja California, *Geol. Soc. Am. Bull.*, **93**, 371-378, 1982.
- Doser, D., Faulting processes of the 1956 San Miguel, Baja California, earthquakes, *Pure Appl. Geophys.*, **139**, 3-16, 1992.
- Frez, J., and V. M. Frias-Camacho, Mapas Anuales de Sismicidad para la region Fronteriza de Ambos California, *Geos. Union Geofis. Mex.*, **AC**, **18**, 112-130, 1998.
- Frez, J., and J. J. Gonzalez, Crustal structure and seismotectonics of northern Baja California, in *Gulf and Peninsular Province of the Californias*, edited by J. Dauphin and B. Simoneit, *AAPG Mem.*, **47**, 261-283, 1991.
- Frez, J., J. J. Gonzalez, J. G. Acosta, F. A. Nava, I. Mendez, J. Carlos, R. E. Garcia-Arthur, and M. Alvarez, A detailed microseismicity study and current stress regime in the Peninsular Ranges of northern Baja California, Mexico: The Ojos Negros region, *Bull. Seismol. Soc. Am.*, **90**, 1133-1142, 2000.

- Govers, R., Dynamics of lithospheric extension: A modeling study, Ph.D. thesis, Utrecht Univ., Utrecht, 240 pp., 1993.
- Hanks, T. C., and H. Kanamori, A moment-magnitude scale, *J. Geophys. Res.*, **84**, 2348–2350, 1979.
- Hill, D. P., and W. Thatcher, An energy constraint for frictional slip on misoriented faults, *Bull. Seismol. Soc. Am.*, **82**, 883–897, 1992.
- Hirabayashi, C. K., T. K. Rockwell, S. G. Wesnousky, M. W. Stirling, and F. Suarez-Vidal, A neotectonic study of the San Miguel-Vallecitos fault, Baja California, Mexico, *Bull. Seismol. Soc. Am.*, **86**, 1770–1783, 1996.
- Humphreys, E. D., and R. J. Weldon, Kinematic constraints on the rifting of Baja California, in *Gulf and Peninsular Province of the Californias*, edited by J. Dauphin and B. Simoneit, *AAPG Mem.*, **47**, 217–229, 1991.
- Ivins, E. R., T. H. Dixon, and M. P. Golombek, Extensional re-activation of an abandoned thrust: A bound on shallowing in the brittle regime, *J. Struct. Geol.*, **12**, 303–314, 1990.
- Johnson, T. L., J. Madrid, and T. Koczyński, A study of microseismicity in Northern Baja California, Mexico, *Bull. Seismol. Soc. Am.*, **66**, 1921–1929, 1976.
- Kenner, S. J., and P. Segall, Post-seismic deformation following the 1906 San Francisco earthquake, *J. Geophys. Res.*, **105**, 13,195–13,209, 2000.
- Lewis, C. J., and J. M. Stock, Paleomagnetic evidence of localized vertical axis rotation during Neogene extension, Sierra San Fermin, northeastern Baja California, Mexico, *J. Geophys. Res.*, **2455**–2470, 1998.
- Li, V. C., and J. R. Rice, Crustal deformation in great California earthquakes, *J. Geophys. Res.*, **92**, 11,533–11,551, 1987.
- Mann, P., F. W. Taylor, R. Edwards, and T. L. Ku, Actively evolving microplate formation by oblique collision and sideways motion along strike-slip faults: An example from the northeastern Caribbean plate margin, *Tectonophysics*, **246**, 1–69, 1995.
- Mao, A., C. G. A. Harrison, and T. H. Dixon, Noise in GPS coordinate time series, *J. Geophys. Res.*, **104**, 2797–2816, 1999.
- Matsu'ura, M., D. Jackson, and A. Cheng, Dislocation model for crustal deformation at Hollister, California, *J. Geophys. Res.*, **91**, 12,661–12,674, 1986.
- Melosh, H. J., and A. Raefsky, The dynamical origin of subduction zone topography, *Geophys. J. R. Astron. Soc.*, **60**, 333–354, 1980.
- Melosh, H. J., and A. Raefsky, A simple and efficient method for introducing faults into finite element computations, *Bull. Seismol. Soc. Am.*, **71**, 1391–1400, 1981.
- Melosh, H. J., and A. Williams, Mechanics of graben formation in crustal rocks: A finite element analysis, *J. Geophys. Res.*, **92**, 13,961–13,973, 1989.
- Miller, M. M., R. E. Crippen, T. H. Dixon, Neotectonic studies of northern Baja California, Mexico, with Landsat Thematic Mapper and SPOT panchromatic imagery: Partitioning of dextral and extensional strain at the Pacific–North America plate boundary, in *Proceedings of the 5th International Colloquium on Physical Measurements and Signatures in Remote Sensing*, *Eur. Space Agency Spec. Publ.*, **SP-319**, 791–796, 1991.
- Ness, G. E., and M. W. Lyle, A seismo-tectonic map of the Gulf and Peninsular province of the Californias, in *Gulf and Peninsular Province of the Californias*, edited by J. Dauphin and B. Simoneit, *AAPG Mem.*, **47**, 71–78, 1991.
- Nur, A., and G. Mavko, Postseismic viscoelastic rebound, *Science*, **183**, 204–206, 1974.
- Okada, Y., Surface deformation due to shear and tensile faults in a half space, *Bull. Seismol. Soc. Am.*, **75**, 1135–1154, 1985.
- Okada, Y., Internal deformation due to shear and tensile faults in a half-space, *Bull. Seismol. Soc. Am.*, **82**, 1018–1040, 1992.
- Pollitz, F. F., Gravitational visco-elastic postseismic relaxation on a layered spherical Earth, *J. Geophys. Res.*, **102**, 17,921–17,941, 1997.
- Pollitz, F. F., and I. S. Sacks, Modeling of postseismic relaxation following the great 1857 earthquake, southern California, *Bull. Seismol. Soc. Am.*, **82**, 454–480, 1992.
- Pollitz, F. F., and I. S. Sacks, Fault model of the 1891 Nobi earthquake from historic triangulation and leveling, *J. Phys. Earth*, **42**, 1–43, 1994.
- Pollitz, F. F., G. Peltzer, and R. Bürgmann, Mobility of continental mantle: Evidence from post-seismic geodetic observation following the 1992 Landers earthquake, *J. Geophys. Res.*, **105**, 8035–8054, 2000.
- Rebollar, C. J., and M. S. Reichle, Analysis of the seismicity detected in 1982–1984 in the northern Peninsular Ranges of Baja California, *Bull. Seismol. Soc. Am.*, **77**, 173–189, 1987.
- Reyes, A., J. Brune, T. Barker, L. Canales, J. Madrid, J. Rebollar, and L. Munguia, A microearthquake survey of the San Miguel fault zone, Baja California, Mexico, *Geophys. Res. Lett.*, **2**, 56–59, 1975.
- Rockwell, T. K., D. L. Schug, and M. E. Hatch, Late Quaternary slip rates along the Agua Blanca fault, Baja California, Mexico, in *Geological Investigations of Baja California*, *South Coast Geol. Soc., Ann. Field Trip Guideb. no. 21*, edited by P. L. Abbott, S. Coast Geol. Soc., Santa Ana, Calif., pp. 53–92, 1993.
- Rosencrantz, E., and P. Mann, SeaMarc-II mapping of transform faults in the Cayman Trough, Caribbean Sea, *Geology*, **19**, 690–693, 1991.
- Rydelek, P. A., and I. S. Sacks, Asthenospheric viscosity and stress diffusion: A mechanism to explain correlated earthquakes, *Geophys. J. Int.*, **100**, 39–58, 1990.
- Savage, J. C., and R. O. Burford, Geodetic determination of relative plate motion in central California, *J. Geophys. Res.*, **78**, 832–845, 1973.
- Savage, J. C., and M. Lisowski, Viscoelastic coupling model of the San Andreas Fault along the big bend, southern California, *J. Geophys. Res.*, **103**, 7281–7292, 1998.
- Savage, J. C., and W. H. Prescott, Asthenosphere re-adjustment and the earthquake cycle, *J. Geophys. Res.*, **83**, 3369–3376, 1978.
- Scholz, C., *The Mechanics of Earthquakes and Faulting*, Cambridge Univ. Press, New York, 439 pp., 1990.
- Shor, G. G., Jr., and E. Roberts, San Miguel, Baja California Norte, earthquakes of February, 1956: A field report, *Bull. Seismol. Soc. Am.*, **48**, 101–116, 1958.
- Sillard, P., Z. Altamimi, and C. Boucher, The ITRF96 realization and its associated velocity field, *Geophys. Res. Lett.*, **25**, 3222–3226, 1998.
- Suarez-Vidal, R., G. Armijo, P. Morgan, R. Bodon, and G. Gastil, Framework of recent and active faulting in northern Baja California, in *Gulf and Peninsular Province of the Californias*, edited by J. Dauphin and B. Simoneit, *AAPG Mem.*, **47**, 285–300, 1991.
- Thatcher, W., Regional variations of seismic source parameters in the northern Baja California area, *J. Geophys. Res.*, **77**, 1549–1565, 1972.
- Thatcher, W., Nonlinear strain buildup and the earthquake cycle on the San Andreas fault, *J. Geophys. Res.*, **88**, 5893–5902, 1983.
- Wdowinski, S., Y. Bock, J. Zhang, P. Fang, and J. Genrich, Southern California permanent GPS geodetic array: Spatial filtering of daily positions for estimating coseismic and post-seismic displacements induced by the 1992 Landers earthquake, *J. Geophys. Res.*, **102**, 18,057–18,070, 1997.
- Wells, D. L., and K. J. Coppersmith, New empirical relationships among magnitude, rupture length, rupture width, rupture area and surface displacement, *Bull. Seismol. Soc. Am.*, **84**, 974–1002, 1994.
- Wessel, P., and W. H. F. Smith, New version of generic mapping tools released, *Eos Trans. AGU*, **76**, 329, 1995.
- Wesnousky, S. G., Seismicity and structural evolution of strike slip faults, *Nature*, **335**, 340–343, 1988.
- Zumberge, J., M. Heflin, D. Jefferson, M. Watkins, and F. Webb, Precise point positioning for efficient and robust analysis of GPS data from large networks, *J. Geophys. Res.*, **102**, 5005–5017, 1997.

R. Bennett, Harvard-Smithsonian Center for Astrophysics, Cambridge, MA, USA.

J. Decaix, T. Dixon, and F. Farina, Rosenstiel School for Marine and Atmospheric Sciences, University of Miami, 4600 Rickenbacker Causeway, Miami, FL 33149-1098, USA. (tdixon@rsmas.miami.edu)

J. Fletcher and F. Suarez-Vidal, CICESE, Ensenada, Mexico.

K. Furlong and R. Malservisi, Geodynamics Research Group, Department of Geosciences, Pennsylvania State University, University Park, PA, USA.

J. Lee, Department of Geological Sciences, Central Washington University, Ellensburg, WA, USA.